The cellular Notch1 Protein Promotes KSHV reactivation in an Rta-dependent manner.

Jennifer DeCotiis-Mauro[a,b]+, Sun M. Han[a,b]+, Helena Mello[a,b], Corey Goyeneche[a,b], Giuseppina Marchesini-Tovar[a,b], Lianhua Jin[a,b], Vivian Bellofatto[a,b], and David M. Lukac[a,b]#

[a] Dept of Microbiology, Biochemistry, and Molecular Genetics, Rutgers Biomedical and Health Sciences, New Jersey Medical School, Rutgers University, Newark, NJ

[b]School of Graduate Studies, Rutgers Biomedical and Health Sciences, Health Science Campus at Newark, Rutgers University, Newark, NJ

Running Head: Notch1 contributes to KSHV reactivation

#Corresponding author: E-mail: Lukacdm@njms.rutgers.edu

+ authors contributed equally to this work

Abstract: 239 words

Abstract

The cellular Notch signal transduction pathway is intimately associated with infections by Kaposi's sarcoma-associated herpesvirus (KSHV) and other gamma-herpesviruses. RBP-Jk, the cellular DNA binding component of the canonical Notch pathway, is the key Notch downstream effector protein in virus-infected and uninfected animal cells. Reactivation of KSHV from latency requires the viral lytic switch protein, Rta, to form complexes with RBP-Jk on numerous sites within the viral DNA. Constitutive Notch activity is essential for KSHV pathophysiology in models of Kaposi's sarcoma (KS) and Primary Effusion Lymphoma (PEL), and we demonstrate that Notch1 is also constitutively active in infected Vero cells. Although the KSHV genome contains >100 RBP-Jk DNA motifs, we show that none of the four isoforms of activated Notch can productively reactivate the virus from latency in a highly quantitative trans-complementing reporter virus system. Nevertheless, Notch contributed positively to reactivation because broad inhibition of Notch1-4 with gamma secretase inhibitor (GSI) or expression of dominant negative mastermind-like1 (dnMAML1) coactivators severely reduced production of infectious KSHV from Vero cells. Reduction of KSHV production is associated with gene specific reduction of viral transcription in both Vero and PEL cells. Specific inhibition of Notch1 by siRNA partially reduces production of infectious KSHV, and NICD1 forms promoter-specific complexes with viral DNA during reactivation. We conclude that constitutive Notch activity is required for robust production of infectious KSHV, and our results implicate activated Notch1 as a pro-viral member of a MAML1/RBP-Jk/DNA complex during viral reactivation.

51 **Importance**

52 Kaposi's sarcoma-associated herpesvirus (KSHV) manipulates the host cell oncogenic Notch
53 signaling pathway for viral reactivation from latency and cell pathogenesis. KSHV reactivation requires
54 that the viral protein Rta functionally interacts with RBP-Jk, the DNA binding component of the Notch
55 pathway, and with promoter DNA to drive transcription of productive cycle genes. We show that the
56 Notch pathway is constitutively active during KSHV reactivation and is essential for robust production
57 of infectious virus progeny. Inhibiting Notch during reactivation reduces expression of specific viral
58 genes yet does not affect growth of the host cells. Although Notch cannot reactivate KSHV alone, the
59 requisite expression of Rta reveals a previously unappreciated role for Notch in reactivation. We
60 propose that activated Notch cooperates with Rta in a promoter-specific manner that is partially
61 programmed by Rta's ability to redistribute RBP-Jk DNA binding to the virus during reactivation.
62

63 **Introduction**

64 Human gammaherpesviral infections and pathogenesis are dependent on interactions of the virus
65 with the cellular Notch signal transduction pathway (1). In uninfected cells, the canonical model of
66 Notch signaling involves activation of the Notch protein by proteolytic release of the Notch Intracellular
67 Domain (NICD)1 from the membrane-associated Notch1 receptor (2, 3). NICD1 then translocates to the
68 cell nucleus, binds to DNA-bound Recombination signal binding protein (RBP)-Jk and activates
69 transcription by displacing a transcriptional co-repressor complex from RBP-Jk and assembling a
70 transcriptional co-activator complex.

71 Reactivation of the gammaherpesvirus Kaposi's sarcoma-associated herpesvirus (KSHV)
72 requires the KSHV Replication and transcriptional activator (Rta) to assemble a complex with RBP-Jk
73 and DNA to activate transcription of essential viral genes (4-27). Reflecting the central roles of Rta and
74 RBP-Jk in reactivation, the KSHV genome contains greater than 100 consensus RBP-Jk DNA motifs,
75 and Rta and RBP-Jk co-occupy many viral promoters during reactivation in B cells (28). However,
76 although both Rta and NICD1 target RBP-Jk, we and others have shown that only Rta is sufficient to
77 productively reactivate KSHV in B cell models of latency (6, 29). Indeed, our recent work showed that
78 ectopic expression of Rta in infected Vero cells induced profound production of infectious virus assayed
79 by a robust and sensitive trans-complementing reporter virus-cell system (30). In parallel experiments,
80 this highly sensitive assay revealed that ectopic expression of NICD1 failed to produce detectable virus
81 (30). Thus, this highly sensitive Vero-cell reactivation system confirmed conclusions from human B cell
82 studies and is ideal to compare transcriptional mechanisms of Rta and Notch because its robustness
83 exceeds those of other infection models.

84 Despite ectopic NICD1's insufficiency to reactivate KSHV alone, the literature suggests that
85 Notch signaling contributes to regulation of KSHV infection. Notch can activate viral productive cycle
86 genes without inducing complete reactivation in B and endothelial cell models of latency (29, 31). In

87 infected primary effusion lymphoma (PEL) cells, conditionally-expressed NICD1 activated a subset of
88 viral genes that were different than those activated by Rta (29). Nevertheless, a broader review of the
89 literature shows that our understanding of Notch's role in KSHV reactivation remains debatable. One
90 study concluded that ectopic NICD1 is capable of inducing complete reactivation (32) by directly
91 activating Rta's promoter and a second study indicated that Notch inhibits reactivation in neighboring
92 cells by indirectly repressing Rta expression (33). The interpretation of experiments intended to analyze
93 the role of Notch signaling in KSHV reactivation are complicated by two observations: first, Notch
94 signaling is constitutively-active in all KSHV-infected cells, and second, one or more of the activated
95 Notch proteins (i.e. NICD1-4) is required for growth and survival of KSHV-infected cells (31, 34-40).
96 Indeed, Notch isoforms 1, 2, and 4, Notch activating ligands, and numerous Notch target genes are
97 overexpressed and active in KS lesional tissue, PEL cells, and in KSHV-infected endothelial cells.
98 Notch signaling is also reciprocally impacted by KSHV infection in myriad and complex ways.
99 The expression of Notch ligands and receptors are increased by specific latent and lytic viral proteins,
100 including Rta, in infected lymphatic endothelial cells (31, 35, 37-39). Notch signaling is reprogramed
101 when the viral immediate early protein Rta stimulates RBP-Jk DNA binding and by proteolytic
102 processing of Notch effector proteins (6, 9, 28, 41). Rta-dependent stimulation of RBP-Jk binding to the
103 KSHV Mta promoter converts it to a Notch-responsive gene (6). Moreover, our ChIP/Seq studies
104 demonstrated that RBP-Jk binding to the viral genome is dramatically redistributed during reactivation,
105 but Rta and RBP-Jk do not co-occupy every newly identified RBP-Jk site (28). Taken together, these
106 data suggest that Notch plays an essential and complementary role with Rta in KSHV reactivation.
107 While it is clear that Rta is the only viral protein that is necessary and sufficient to reactivate the
108 complete KSHV lytic cycle, a complete understanding of Rta's reactivation function must consider the
109 intracellular environment that is replete with potent, constitutive Notch activity.

110 In the present study, we use the KSHV-infected Vero cell model and multiple complementary
111 methodologies to demonstrate that Notch signaling is key to viral reactivation. Specifically, we
112 demonstrate that exposing infected cells to the Notch small-molecule-inhibitor DAPT, or to Notch-
113 inhibiting dominant negative Mastermind-like (dnMAML)-1, severely reduces production of infectious
114 KSHV, after either chemical induction of virus or forced expression of Rta. Inhibition of KSHV virion
115 production is accompanied by reduction of selected viral transcripts and proteins. Importantly,
116 reactivation stymied by DAPT treatment is not the result of cell growth reduction by the drug. While we
117 show that none of the four Notch isoforms are sufficient to reactivate the virus, transfection of specific
118 siRNAs implicates Notch 1 as one of the isoforms that contribute to Rta-induced reactivation. We
119 observe formation of specific Notch1/DNA complexes on the viral genome during reactivation. Finally,
120 we also observe a block in reactivation, which is measured here by a decrease in viral DNA production,
121 by inhibiting Notch in naturally KSHV-infected PEL cells. Taken together, our study illustrates that
122 although Rta is necessary and sufficient for KSHV reactivation, viral reactivation relies on continued
123 endogenous Notch signaling, likely by working with Rta cooperatively during the early steps of
124 reactivation.
125
126
127

128 **Materials and Methods**

129

130 **Plasmids:** All plasmids were grown in DH5α *E. coli* and purified using the cesium chloride maxi-prep
131 method (42). All prepared plasmids were confirmed via restriction enzyme digestion and/or sequencing.
132 pcDNA3-FLg50 expresses full length Rta protein from a genomic allele of KSHV ORF50 (43).
133 pCAGGS:dnMAML1-GFP and pEGFP-N1-dnMAML1 express dominant negative mutants of MAML1
134 fused to GFP and were gifts of Dr. Signe V. Horn Pederson (44). pEGFP-N1-H2b (referred to as H2b-
135 GFP) expresses GFP-fused histone H2b and was a gift of Dr. Geoff Wahl (Addgene plasmid #11680)
136 (45). pcDNA3.1-HisLacZ (13) expresses β-galactosidase reporter protein under control of the HCMV
137 enhancer. The reporter plasmids 4xCSL-luciferase (Addgene plasmid #41726) and 4xCBS-luciferase
138 encode firefly luciferase under the control of four RBP-Jk binding sites are were gifts of Dr. Raphael
139 Kopan and Dr. Rhett Kovall, respectively (46, 47). p3xFLAG-NICD 1-4 express Notch intracellular
140 domains (NICD) 1-4 from the p3xFLAG-CMV-7 expression vector and were gifts of Dr. Raphael
141 Kopan (48). pCMV-NICD1 and pCMV-NICDΔPEST express WT and PEST-domain-deleted alleles of
142 NICD1, respectively, and were gifts of Tom Kadesch. pcDNA3.1-ORF50ΔSTADV5 expresses
143 transcriptionally inert, dominant negative KSHV Rta (nts 1-1590) fused to the V5 epitope tag (13).
144 pCMV-NICD1-P12 and NICD1-L1594P express NICD1 alleles containing different activating
145 mutations found in human T cell acute lymphoblastic leukemia lymphoma cells provided by Dr. Jon C.
146 Aster (49). pcDNA3 (Invitrogen) was used as an empty vector control ("Vec") and DNA filler for all
147 experiments.

148

149 **Cell Culture:** 293 MSR-tet OFF and Vero rKSHV.294 cells (gifts of Dr. Jeff Vieira) were maintained
150 as previously described (30, 50). BC3 cells (a gift of Dr. Ethel Cesarman) and BCBL-1 cells were
151 maintained in RPMI medium supplemented with 12% or 10% Fetal Bovine Serum (FBS) respectively,
152 1% glutamine, 50uM β-mercaptoethanol, and 1% penicillin/streptomycin.

153 Viral reactivation was induced chemically by treatment of cells with 1 mM Valproic acid (VPA;
154 Sigma, P4543; prepared in dH_2O and filtered through 0.22uM surfactant-free cellulose acetate (SFCA)).
155 Notch activity was inhibited chemically by treatment of cells with (2*S*)-*N*-[(3,5-
156 Difluorophenyl)acetyl]-L-alanyl-2-phenyl]glycine 1,1-dimethylethyl ester (DAPT; Selleckchem,
157 S2215); concentrations are given in the figure legends. The solvent vehicle for DAPT was dimethyl
158 sulfoxide (DMSO), which was used as the control, vehicle ("Vh") treatment in all experiments.
159
160

161 **Transfections:** Vero rKSHV.294 cells were plated at a concentration of $2x10^5$ cells per well of 6-well
162 plates and incubated at 37°C overnight. The following day, 2.5 ug of total plasmid DNA and 5 uL of
163 vortexed TransIT-LT1 reagent were added to 250 uL incomplete DMEM and incubated at RT for 30m.
164 The mixture was added to the Vero rKSHV.294 cells dropwise, and cells were incubated for 48 or 72h at
165 37°C, for protein harvest or SeAP assay respectively. Specific plasmids used in transfections are
166 indicated in respective figure legends.
167 For siRNAs, Vero rKSHV.294 cells were plated at a concentration of $2x10^5$ cells per well of six-
168 well plates and incubated overnight at 37° C. The following day, 30 pmol of either control siRNA-A
169 (Santa Cruz, sc-37007), Notch 1 siRNA (h) A (Santa Cruz, sc36095A), or Notch 1 siRNA (h2) (Santa
170 Cruz, sc-44226A) were diluted in 150 uL of incomplete DMEM and mixed with 9 uL of Lipofectamine
171 RNAiMAX reagent previously diluted in incomplete DMEM per manufacturers' suggestions. The
172 mixtures were incubated for 5m at RT, then added to cells.
173

174 **Secreted Alkaline Phosphatase (SeAP) Assay:** Virus-containing media from Vero rKSHV.294 cells
175 were transferred to 293 MSR-tet-OFF cells previously plated at a density of $2x10^5$ cells/well in 6-well
176 plates 24h earlier. 293 MSR-tet-OFF cells were returned to the incubator for 72h (unless otherwise
177 indicated) at 37°C. SeAP-containing media were harvested, and 20 or 25 uL were assayed using either

178 the Great EscAPe SeAP kit (Takara/Clontech) or the Phospha-Light System (Applied Biosystems).
179 Individual data points show results from duplicate, triplicate or quadruplicate technical replicates from
180 one to ten biologic replicates in each figure.
181
182 **Protein extractions and assays**: Cells were washed with 1x PBS, and lysed using RIPA buffer (150
183 mM NaCl, 1% NP40, 0.5% sodium deoxycholate, 0.1% SDS, 50 mM Tris pH 8.0) supplemented with
184 protease inhibitor cocktail (Sigma P2714) and 1 mM DTT. Dishes were scraped, contents were
185 transferred to microfuge tubes, debris was pelleted by centrifugation, and supernatants were transferred
186 to new microfuge tubes. Total protein concentrations were determined by Protein Assay (Bradford; Bio-
187 Rad).
188 For luciferase and β-galactosidase quantitation, at 48h post-transfection, cells were washed twice
189 with 1x PBS, then lysed in 125 uL 1x reporter lysis buffer (Promega) for 20min at RT. Dishes were
190 scraped, contents were transferred to microfuge tubes, debris was pelleted by centrifugation, and
191 supernatants were transferred to new microfuge tubes. Luciferase activity was measured in the BD
192 monolight 3010 luminometer (BD Biosciences) using 20 uL of each extract into which 20 uL luciferase
193 assay substrate was injected (Promega). β-galactosidase activity was measured by absorbance at 420 nm
194 in the Tecan Genios plate reader using 30 uL of each extract mixed with 30 uL of 2x Assay Buffer
195 (Promega).
196
197 **SDS-PAGE and Western Blotting:** Equal amounts of protein, as determined by Bradford Assays, were
198 mixed with 6x Laemmli buffer containing freshly added β-mercaptoethanol, heated at 95°C for 5m, then
199 loaded on gels. Proteins were transferred via electroblotting to nitrocellulose (Main Manufacturing
200 LLC) or PVDF (GVS Filter Tech 1212783; PVDF membranes only were initially dipped in 100%
201 methanol). Membranes were blocked with 5% milk in 1x PBS/0.1% Tween 20 (blocking buffer) for at

202 least 30m, then washed with 1x PBS/0.1% Tween 20 and 1x PBS. Primary antibodies were diluted in
203 blocking buffer then incubated with the blots for 4h at RT or overnight at 4°C; antibodies and dilutions
204 were as follows: anti-Notch1 (1:200, Santa Cruz sc-32745, or bTAN20 Developmental Studies
205 Hybridoma Bank, deposited by Dr. Spyros Artavanis-Tsakonas), anti-Rta (1:4000, D3861 (14)), anti-
206 FLAG (1:1000, M2 Sigma Aldrich F1804, or PA1-984B Thermo scientific), anti-GAPDH (1:1000,
207 BioLegend 919501), anti-GFP (1:200, B-2 Santa Cruz sc-9996) anti-ORF59 (1H10; (14)), anti-KbZIP
208 (51) or anti-histone H3 (1:4000 Proteintech 17168-1-AP), and anti-Mta (52). The membranes were
209 then washed with 1x PBS/0.1% Tween 20 and 1x PBS and incubated for 30m with secondary antibodies
210 diluted in blocking buffer; antibodies and dilutions were as follows: Goat anti-Mouse IgG-h+1 HRP
211 conjugated (1:5000, Bethyl Labs A90-116P), Rabbit TruBlot anti-Rabbit IgG (1:1000, Rockland 18-
212 8816-33), Goat anti-Rabbit IgG-h+1 HRP conjugated (1:5000, Bethyl A120-101P). Membranes were
213 partially dried and incubated for up to 2m in Pierce ECL Western Blotting Substrate (Thermo Scientific,
214 32016). Signals were detected by exposure to autoradiography film (Denville, E3012) for up to 24h, or
215 digitally captured using myECL imager (Thermo Scientific) or Chemidoc (BioRad).
216
217 **Quantitative Reverse Transcription-real-time Polymerase Chain Reaction (RT-qPCR)** Total RNA
218 was extracted from Vero rKSHV.294 cells using the RNeasy kit (Qiagen) as per manufacturer's
219 suggestions. DNA contamination was removed using the TURBO DNA-free kit (Invitrogen) as per
220 manufacturer's suggestions. Transcripts were quantitated by qRT-PCR using the iTaq Universal SYBR
221 Green One-Step Kit (Bio-Rad) following manufacturer's suggestions. 5 to 100 ng. of input RNA was
222 amplified using KSHV-specific unique coding sequence primers (53) or β-actin primers (54) in a
223 CFX96/C1000 instrument (Bio-Rad). Reaction conditions were 10 mins 50ºC for RT, 1 min 95ºC, then
224 40 cycles of 10 sec 95ºC/10 sec 60ºC. Amplification specificity was confirmed for all primer pairs by
225 melt-curve analysis and parallel control reactions that lacked template RNA or reverse transcriptase.

226

227 **vDNA quantitation:** BC3 cells were treated with indicated chemicals for 65h and total DNA was
228 purified from cell lysates using the FlexiGene DNA kit (Qiagen). Intracellular viral DNA was measured
229 by real-time quantitative (q) PCR of the viral genome; GAPDH was the internal control. qPCR reactions
230 were performed using SYBR Green PCR Master Mix (Thermo Scientific). Input DNA (100 ng) was
231 amplified by incubating at 50°C for 10m and 95°C for 10m, then cycled 39 times with melting at 95°C
232 for 15 sec and annealing at 60°C for 1m. Fold DNA was calculated using the ΔCt method and all values
233 were normalized to that of VPA + vehicle, which was set to 100%.

234

235 **Immunofluorescence**: Cells were harvested in 15 mL conical tubes, washed twice with 1x Phosphate
236 Buffered Saline (PBS), and resuspended at a density of $1.25x10^6$ cells/mL in 1x PBS. 15-20 mm circles
237 were drawn on glass microscope slides with a Super PAP pen (ThermoFisher 008899), then coated by a
238 10m incubation with 4 uL poly-L-lysine. Polylysine was removed, 200 uL of cells/circle were adhered
239 for 30m, then fixed in pre-chilled methanol/acetone (50/50 v/v) at -20°C for 5 to 10min. Slides were air
240 dried for 10min at RT and cells were blocked with 3% BSA/1% glycine in 1x PBS. The following
241 primary antibodies were diluted in 1:1000 in blocking buffer and incubated for 1h with the cells: anti-
242 Rta (D3861; (14)), anti-K8.1 (Santa Cruz Bio sc-65446, 1:1000), or anti-ORF59 (1H10; (14)). Cells
243 were washed with 1x PBS/0.4% Tween20 and 1x PBS, then the following secondary antibodies were
244 diluted 1:500 in blocking buffer and incubated for 1h with the cells: anti-rabbit DyLight 448 (Thermo
245 Scientific, 35552), anti-rabbit DyLight 550 (Thermo Scientific, 84541), or anti-mouse DyLight 550
246 (Thermo Scientific, 84540). Cells were re-washed, and coverslips were mounted to slides using Vecta-
247 shield with DAPI (Vector Labs).

248

249 **Cell Growth Quantitation:** Vero rKSHV.294 cells were plated at a density of 6.7 x 10^3 cells/well of a
250 96-well dish. 24 h later, cells were treated with 1 uL vehicle alone (control) or containing DAPT (final
251 concentration of 1 or 5 uM), in triplicate. Three mock wells were also prepared with media only for
252 each time point. At the post-treatment times indicated, cell media was replaced with 200 uL growth
253 assay media (180 uL DME + 20 uL Alamar Blue (BioRad BUF012A), and incubation was continued for
254 4 hr at 37°C. Alamar Blue fluorescence was measured by excitation at 544 nm/emission at 590 nm in a
255 SpectraMax M2 plate reader (Molecular Devices). Mock values were averaged and subtracted from
256 each experimental value to yield corrected values. All corrected values were then normalized to 0h
257 values that had been set to the relative value of 1 for each treatment.

258 **Chromatin Immunoprecipitation (ChIP)/Polymerase Chain Reaction (PCR):** Modified from (55,
259 56). Vero rKSHV.294 cells were plated at (1.5x10^6 cells per 100mm plate). 24h later, cells were
260 transfected in triplicate with 12.5 ug total of pcDNA3 or pcDNA3-FLg50 using TransIT LT1 (Mirus)
261 per manufacturer's protocol. 24h after transfection, chromatin was cross-linked by replacing growth
262 medium with 8 mL of serum-free medium containing 1.42% methanol-free formaldehyde (Peirce) and
263 incubating for 8m at room temperature. Formaldehyde was quenched with 125 mM glycine for 5m at
264 room temperature, then washed twice with 10 mL ice cold 1x PBS. Cells were scraped into fresh 10 mL
265 of ice cold 1x PBS, transferred to 15 mL conical tubes, and combined with an additional 2 mL of 1x
266 PBS that was used to rinse residual cells from each plate. Cells were pelleted by centrifugation at
267 2000g, 5m, at 4° C. Pellets from single plates were lysed by resuspension in 1 mL of ChIP buffer (150
268 mM NaCl, 50 mM Tris-HCl (pH 7.5), 5 mM EDTA, 0.5% v/v NP-40, 1.0% v/v Triton X-100), and
269 supplemented with protease inhibitor cocktail (Sigma P2714) by repeated slow-pipetting after transfer to
270 1.5 mL Bioruptor Micro tubes (Diagenode) on ice. Incubation on ice was continued for 10m, and

271 nuclear pellets were recovered by centrifugation at 12,000g for 1m at 4° C. Nuclear pellets were
272 resuspended in 300 uL sonication buffer (ChIP buffer plus 1.0% v/v Sodium dodecyl-sulfate), and
273 chromatin sonicated in the Bioruptor Pico (Diagenode) to average size of 250 bp (typically 15 cycles of
274 30s on/30s off, vortexing every 5 cycles). Nuclear lysates were as cleared by centrifugation at 12,000g,
275 10m, 4° C, and aliquoted in 2 million cell equivalents per subsequent ChIP. Some chromatin was set
276 aside for analysis of input quality and quantity.

277 ChIPs were performed by adding anti-NICD1 antibody (Cell Signaling 3608) or equal amounts
278 of non-specific rabbit IgG (Sigma PP64) to individual chromatin aliquots: 0.55 or 1 ug of each antibody
279 were added to 1 million or 2 million cell equivalents, respectively. ChIPs were incubated 16-24h at 4° C
280 with nutation. Chromatin was cleared by centrifugation at 12000g for 10 mins at 4° C and mixed with
281 magnetic Protein A/G beads (Cytiva 17152104010150) that had been prewashed with ChIP buffer and
282 blocked with ChIP buffer/1% v/v Bovine Serum Albumin. ChIP'd chromatin was recovered by
283 incubating with beads for 45m at 4° C with nutation. Beads were washed 6 times with 1 mL each of
284 ChIP buffer on a magnetic tube rack (Invitrogen). After removing the final wash, DNA was recovered
285 by resuspending the magnetic beads in 100 uL 10% w/v Chelex 100/d$H_2$0 suspension (Bio-Rad) and
286 boiling the mixture for 10m. After cooling, proteins were removed by adding 20 ug of Proteinase K,
287 vortexing, and incubating on a thermal mixer at 55° C for 30m at 1000 rpm. Proteinase K was
288 inactivated by boiling samples for 10m, then centrifuged for 1m at 12000g, 4° C. 80 uLs of supernatant
289 was transferred to new tubes. Fresh 120 uLs of dH_2O was added to the Chelex resin, vortexed for 10s,
290 and centrifugation repeated. 120 uL of that supernatant was removed and mixed with first 80 uL aliquot.

291 Purified DNA was analyzed using real-time qPCR with SYBR green (Applied Biosystems
292 4472918); primer sequences are available upon request. Fold enrichment of NICD1 on vDNA was
293 calculated using the ΔΔCt method, comparing the Ct for anti-NICD1 to IgG first for each sample, then

294 EV to Rta-transfected samples second. Final folds were determined by scaling to input chromatin and
295 amount of NICD1 expression in each condition. Data shown represent results of four independent
296 transfections performed in duplicate or triplicate, and ChIP'd twice per transfection. Two ChIPs from
297 one transfection used alternate control non-specific IgG (Cell Signaling 2729S) or anti-GFP (Cell
298 Signaling 2956) to confirm results.

299

300 **Statistical Analyses:** Outlying data points in each experiment were identified using Peirce's
301 criterion and eliminated from final quantitation and graphs (57).

302 **Results**

303 **Notch1 is constitutively active in KSHV-infected Vero cells**

304 To understand the complex interactions of Notch signaling with KSHV infection, we have
305 employed an infected Vero cell model. These cells have emerged as a robust system for understanding
306 host and viral regulation of productive KSHV reactivation. Infected Vero cells provide a number of
307 improvements over other reactivation models, including their ease of transfection. Gantt and colleagues
308 (50) developed a Vero cell line that produces a recombinant KSHV reporter virus upon reactivation that
309 is quantifiable by infecting a trans-complementing 293 cell line. Using this system, we previously
310 demonstrated that ectopic, activated Notch1 (NICD1) was insufficient to produce infectious virus,
311 confirming work from studies of PEL cells (6, 29, 30).

312 Many cellular models of KSHV infection demonstrate constitutive activation of NICD1 (31, 34,
313 36-38) which is required to maintain cell growth and survival (36-38). Based on the dramatic
314 association of Notch activity with KSHV infection in those cells, we sought to determine the status of
315 Notch1 in infected Vero cells. We prepared total protein extracts from infected Vero cells. Western
316 blotting with anti-Notch1-specific antisera demonstrated a protein band doublet that migrated with an
317 apparent molecular weight (MW) of 100-120 kDa (Fig. 1A). The upper band matched the migration of
318 the band observed from control, uninfected Vero cells transfected with an NICD1 expression vector
319 (Fig. 1A). Therefore, we conclude that Notch1 is constitutively active in latent, KSHV-infected Vero
320 cells. Interestingly, significantly-less activated Notch1 is observed in uninfected Vero cells (center lanes
321 of Fig 1A, quantitated in Fig 1B). These data suggest that latent infection of Vero cells reduces
322 activation of endogenous Notch1. However, we can't exclude the possibility that the reduction of
323 Notch1 activation trivially results from the Puromycin selection of the virus episome in rKSHV.294
324 cells. Others have shown that expression of one or several productive cycle KSHV proteins could
325 induce expression of Notch pathway components in 293 cells (39).

326

327
328
329 **Inhibiting Notch activation reduces KSHV reactivation**

330 To determine whether endogenous, constitutive Notch activity contributed to KSHV reactivation,
331 we measured the effect of DAPT treatment on mature infectious virus production from Vero
332 rKSHV.294 cells. Cells were pre-treated with DAPT or the vehicle control ("Vh"; DMSO) for 24h, then
333 transfected with Rta expression vector to induce viral reactivation or empty vector (Vec) control. When
334 Notch is active, which is the case in the Vh only cultures, ectopic Rta reactivates virus to approximately
335 700-fold greater than Vec, as we previously published (Fig. 2A) (30). In cells where Notch is inhibited,
336 which is the case in the DAPT-treated cells, and viral reactivation is attempted by Rta addition,
337 reactivation is stymied. These data suggest that constitutive Notch activity is necessary for optimal viral
338 production (Fig. 2A).

339 Since reactivation is scored by transferring the supernatants from the infected Vero cells to 293
340 MSR tet-OFF cells, we performed a key control experiment to assess the potential effect of DAPT on
341 the function of the 293 reporter cells. We treated virus-containing supernatant media from the
342 experimental Vero rKSHV.294 cells with DAPT prior to incubating the supernatants with the 293 cells.
343 There was no decrease in virus detection in the 293 cells, confirming that DAPT does not inhibit *de*
344 *novo* infection by KSHV nor expression of the SEAP reporter protein (Fig S1).

345 To confirm that NICD activity was reduced by DAPT treatment in the infected Vero cells, we co-
346 transfected the Vero rKSHV.294 cells with two reporter plasmids. One contained four RBP-Jk motifs
347 arrayed in tandem upstream of a luciferase reporter gene, and the other contained the HCMV enhancer
348 sequence lacking RBP-Jk motifs for normalization. As expected, treatment of the cells with 5 uM
349 DAPT for 6 or 24h reduced Notch activity relative to vehicle-treated cells (Fig. 2B).

350 To determine if viral gene expression was similarly debilitated by inhibiting Notch activation
351 during reactivation, we measured levels of viral transcripts in the infected Vero cells. We observed a
352 gene specific reduction in viral RNAs (Figs 2C and D) in cells where Notch is inhibited (+DAPT) and
353 viral reactivation is induced by ectopic Rta. The expression of K2, ORF74, ORF8, ORF6, ORF34, and
354 K8.1 transcripts were significantly reduced by inhibiting Notch transactivation with DAPT (Figs 2C and
355 D). ORF6 and ORF55 transcripts followed the same trend of sensitivity to Notch inhibition, but did not
356 reach statistical significance (Fig 2D). K14 transcript was activated by Rta expression but not reduced
357 by Notch inhibition, and ORF72 transcription was neither induced by Rta expression or repressed by
358 DAPT pre-treatment (Fig 2C). We conclude that activated Notch cooperates with Rta to support
359 production of infectious KSHV by transactivating specific, essential viral genes.
360
361 **Inhibiting Notch activation does not reduce growth of KSHV-infected Vero cells**
362 Notch inhibition by DAPT can inhibit growth and induce apoptosis in KSHV-infected cells (31,
363 34-40). To determine the effect of DAPT on growth of the infected Vero rKSHV.294 cells, we
364 measured cell viability by alamarBlue sensitivity. Over a 72h period of growth, cells treated with 1 uM
365 or 5 uM DAPT maintained normal cell viability (Fig. 2E). The Fig. 2 data therefore support the
366 conclusion that Notch inhibition by DAPT treatment specifically reduces viral reactivation without
367 affecting Vero cell growth or viability.
368
369 **Inhibiting the Notch transactivation complex reduces KSHV reactivation**
370 Inhibiting the gamma-secretase complex with DAPT can block the formation of several signaling
371 substrates in addition to Notch (58). Therefore, we worked to specifically block Notch activity directly
372 at its site of transcriptional transactivation by testing the effects of ectopically expressing dominant
373 negative (dn) mutants of the Mastermind-like1 (MAML1) protein. Cognate MAML1 stabilizes the

374 NICD1/RBP-Jk/DNA complex to facilitate NICD1-dependent transactivation in the nucleus (2, 3, 59,
375 60). Transfection of Vero rKSHV.294 cells with two different dnMAML1 expression vectors reduced
376 Rta-mediated reactivation by 40% or 90%, respectively (Fig. 3A). As a control, we observed that
377 dnMAML1 proteins were strongly expressed (Fig 3B).
378 To determine if viral gene expression was similarly debilitated by inhibiting the Notch
379 transactivation complex during reactivation, we measured protein levels in the infected Vero cells. We
380 observed a gene specific reduction in viral proteins (Figs 3C and D) in cells expressing dnMAML1
381 relative to empty vector-transfected cells. The expression of Mta and KbZIP proteins were significantly
382 reduced by inhibiting Notch transactivation with dnMAML1. ORF59 induction was also reduced by
383 Notch inhibition in the single protein samples tested. Taken together with Fig 2, we conclude that
384 activated Notch supports production of infectious KSHV by transactivating specific, essential viral
385 genes in cooperation with Rta.
386
387 **Notch1 is necessary for optimal viral reactivation**
388
389 The data in Figs. 2 and 3 show that inhibiting Notch post-translationally at two different
390 biochemical steps of its activation dramatically reduced KSHV reactivation and support a pro-viral role
391 for Notch signaling in viral reactivation in Vero cells. However, these experiments do not specify which
392 of the four Notch receptors, Notch1,2,3 or 4, are required for efficient reactivation, as all four proteins
393 are inhibited by DAPT and ectopic dnMAML1 (2, 59, 61-65).
394 Since Notch1 is constitutively active in Vero cells, we asked whether specific knock-down of
395 Notch1 would affect viral reactivation. We transfected two different siRNAs to knock-down
396 endogenous Notch1 in Vero-rKSHV.294 cells, and then induced viral reactivation by transfection of Rta
397 expression vector (Fig. 4A) or treatment with the HDAC inhibitor valproic acid (VPA; eg. the most
398 potent chemical inducer of viral reactivation in Vero cells (66)) (Fig. 4B). The Notch1-specific siRNAs

399 reduced viral reactivation up to a maximum of ~80% inhibition ("N1-B" in Fig. 4A) relative to control,
400 scrambled siRNA ("Scr"). Knock-down of NICD1 prior to VPA treatment also reduced production of
401 virus, but did not reach statistical significance in the small number of samples tested (Fig 4B). Knock-
402 down of endogenous Notch1 was confirmed via Western blot (Fig 4C). These data verify that
403 constitutively active Notch1 plays a pro-viral role in KSHV reactivation in Vero cells.
404

405 **Activated Notch1 associates with viral promoter DNA during KSHV reactivation.**
406
407 Our observations that inhibiting Notch during KSHV reactivation reduced viral gene
408 transcription without affecting cell growth (Figs. 2 and 3) suggested that our observed proviral function
409 of Notch1 (Fig 4) is to transactivate specific viral genes to support KSHV reactivation. Activated
410 Notch1 (NICD1) transactivates specific cellular genes by assembling NICD1/MAML1/RBP-Jk1/DNA
411 complexes on promoters or enhancers (2, 3, 59, 60). We and others have demonstrated that RBP-Jk1
412 binds to many sites on KSHV DNA (4-27), and we have mapped eighty-two RBP-Jk1 binding sites to
413 the viral genome during reactivation (55). We selected six of these RBP-Jk1 binding sites found within 1
414 kb upstream of transcription start sites for KSHV genes, ie. in their presumptive promoters, and asked
415 whether we could also detect NICD1 occupancy there using chromatin immunoprecipitation. When we
416 induced reactivation in rKSHV.294 cells by transfecting Rta expression vector, qPCR showed that
417 NICD1 antibody co-precipitated significantly more promoter DNA than in EV-transfected cells on the
418 K2, ORF34, ORF6, ORF8, and the bidirectional ORF50AS/K8 promoters (Fig. 5). Transcription of four
419 of these genes was significantly impaired when Notch activity was inhibited (Figs 2C and D). We
420 conclude that NICD1 forms complexes with RBP-Jk and DNA to transactivate specific viral genes to
421 promote KSHV reactivation.
422
423
424

425 **Notch is pro-viral in PEL cells**
426
427 Notch1 is constitutively active in PEL cells (36-38). To determine whether Notch1 also supports
428 reactivation in these cells, we reactivated virus with VPA in the presence of 16, 32, or 40 uM of DAPT
429 and quantitated vDNA accumulation and protein expression. DAPT reduced intracellular vDNA
430 accumulation up to a maximum of ~80% relative to VPA plus vehicle control ("Vh") (Fig 6A). DAPT
431 also reduced the percentage of K8.1-positive cells (Fig. 6B); as K8.1 is a true-late gene, this result was
432 consistent with the effect of DAPT on vDNA accumulation.
433 Interestingly, we did not observe an effect of DAPT treatment on the percentage of ORF59-
434 positive cells, perhaps because this immunofluorescence assay in PEL cells fails to detect modest effects
435 on the ORF59 amounts or signal intensity (Fig 6B). In Vero cells, western blotting suggested that Notch
436 inhibition reduced overall ORF59 protein expression (Fig 3D).
437 In an SLK cell model of KSHV infection, Notch was shown to inhibit reactivation and reduce
438 expression of productive cycle genes, including Rta (33). In contrast, we did not observe a statistically
439 significant effect of DAPT treatment on Rta expression in any of the experiments we performed in
440 Vero and PEL cells (J. Decotiis-Mauro and D.M. Lukac, unpublished data). Therefore, based on the DE
441 kinetics of expression of many of the Notch-sensitive viral genes (Figs 2, 3, 5, and 6), we conclude that
442 Notch cooperates with Rta to promote reactivation at an early time point that precedes vDNA
443 replication.
444
445 **Ectopic, activated Notch isoforms 1 to 4 are insufficient to reactivate KSHV from latency**
446 In our experiments using the infected Vero cell system, as well as experiments in PEL cells, we
447 demonstrated that ectopic NICD1 is incapable of productively reactivating KSHV, despite widespread
448 RBP-Jk binding to the latent viral genome (6, 9, 30). Mammals express four Notch receptors; although

449 other Notch isoforms are commonly constitutively-expressed in KSHV-infected cells (31, 34, 36-38) it
450 is possible that their endogenous levels are insufficient to drive viral reactivation.

451 Notch receptors 1 to 4 encode all of the functional domains present in NICD1, except for Notch3 and 4,
452 which lack the Notch transactivation domain (reviewed in (2, 67, 68)). Importantly, all four NICDs contain the
453 RBP-Jk-interaction domain and activate promoters containing RBP-Jk DNA motifs. Target selectivity of each
454 NICD differs based on promoter contexts of the RBP-Jk motifs and the cellular contexts in which each receptor is
455 activated (2, 48, 68-80). The sequences and arrangement of RBP-Jk motifs in individual promoters
456 determine the magnitude of transactivation by particular NICD proteins. Moreover, since each Notch
457 receptor can cross-talk with other signaling pathways and transcription factor networks, the co-
458 occupancy of promoters with particular NICD/RBP-Jk complexes and heterologous transcription factors
459 can also determine the responsiveness of a gene to a specific Notch receptor and its respective NICD.

460 To test whether ectopic Notch isoforms 2, 3, and 4 could reactivate KSHV, we transfected
461 vectors that express NICD 2, 3, and 4 into Vero rKSHV.294 cells. As expected, ectopic Rta, the
462 positive control, gave a 500-fold increase in KSHV reactivation as measured by SeAP activity (Fig. 7A).
463 However, little to no virus was detectable from cells transfected with any of the NICD expression
464 vectors, similar to effects in cells transfected with the Rta transcriptionally deficient mutant
465 ORF50ΔSTAD (1.7-fold; Fig. 7A). All four isoforms were thus insufficient to reactivate KSHV from
466 Vero cells, despite their robust expression levels (Fig 7B).

467

468 **Ectopic NICD1 and 2 are transactivation competent in KSHV-infected Vero cells**

469 It is possible that the activated Notch proteins are unable to reactivate KSHV because they are not
470 transcriptionally active in Vero rKSHV.294 cells. To assess their activities, we co-transfected Vero
471 rKSHV.294 cells with a reporter vector containing four tandem RBP-Jκ sites, and each of the four NICD
472 expression vectors at the same amounts as in Fig 7A. We observed significant transactivation of this
473 promoter by both NICD1 and 2, but not NICD3 or 4 (Fig 7C). Taken together with Fig. 7A, these data

474 confirm that NICD1 and 2 are incapable of reactivating KSHV despite being transcriptionally active.
475 However, the inability of NICD3 or 4 to activate transcription in these cells provides a potential
476 explanation for their inability to reactivate KSHV from latency.
477
478 **NICD mutants of varying activity are insufficient to reactivate KSHV from latency**
479 NICD1 dosage has dramatic effects on biologic phenotypes. Since endogenous, constitutively-
480 active Notch1 is abundant in the infected Vero cells (Fig 1), it was possible that ectopic NICD1 failed to
481 reactivate KSHV (Fig 7A) due to excessive Notch activity. To vary the gain-of-function activity of
482 Notch1 in the infected Vero cells, we expressed a set of four Notch1 alleles known to have varying
483 intrinsic signaling and transactivating potencies. Notch1-P12 and Notch1-L1594P, identified in clinical
484 T cell acute lymphoblastic leukemia (T-ALL) lymphomas, are full-length Notch1 receptors expressed
485 from the pCMV vector that each produce constitutively-active NICD1 due to mutations in the Notch1
486 heterodimerization domain that promote cleavage of the mutant proteins (49, 81)(Fig S2A). Both
487 Notch1 mutants are weaker transcriptional transactivators than WT pcDNA3-NICD1, which expresses
488 NICD1 lacking the transmembrane domain and protease cleavage sites and bypasses the requirement for
489 proteolysis to generate the active NICD1 transactivator (49, 81). The fourth clone, pCMV-NICD1-
490 ΔPEST, expresses a mutant of NICD1 protein that also lacks the PEST proteasomal degradation domain,
491 conferring increased stability to NICD1 and stronger, more sustained transactivation. We transfected
492 vectors expressing each of these alleles into the Vero rKSHV.294 cells and found that none could
493 reactivate the virus, similar to the result with cognate NICD1 ("WT"; Fig S2B). These data further
494 verify that NICD1 is insufficient to reactivate KSHV from latency, regardless of its inherent potency or
495 expression level.
496
497 **NICD1 cooperates with VPA in reactivation**

498 Our data showed that endogenous Notch1 is constitutively active in infected Vero cells and
499 supports optimal viral reactivation that is induced by VPA treatment or by ectopic Rta expression.
500 However, increasing activated Notch1 amounts alone, via ectopic NICD1 expression, was insufficient to
501 productively reactivate KSHV (Figs 7 and S2). To determine whether ectopic NICD1 could cooperate
502 with VPA treatment, we transfected the Vero rKSHV.294 cells with the NICD1 expression vector alone
503 or with 1 mM VPA treatment. In positive control samples treated with VPA alone, we observe
504 approximately 350-fold reactivation (Fig 8). As expected, ectopic expression of NICD1 alone was
505 insufficient to produce virus (Fig 8). However, expression of ectopic NICD1 in VPA-treated cells
506 significantly enhanced reactivation to about 700-fold (Fig 8), supporting a cooperative role for NICD1
507 and VPA. The NICD1 mutants, NICD1ΔPEST, P12, and L1594P, also increased VPA-stimulated
508 reactivation, but did not reach statistical significance due to the small sample size (Fig S2C).
509
510

511 **Discussion**

512 In this work, we demonstrate that ectopic expression of activated Notch1 is insufficient to
513 productively reactivate KSHV from latency (Fig 7). NICD1's reactivation insufficiency confirms our
514 earlier results from ectopic expression of NICD1 in PEL and Vero cells (6, 30), and agrees with similar
515 results in which NICD1 was conditionally-induced ectopically in a stably-transfected PEL cell line (29).
516 To ensure that this negative result is not due to an inadequate dose of ectopic NICD1, we show that three
517 additional Notch1 alleles that encode constitutively active NICD1 proteins with varied intrinsic
518 transcriptional potency also fail to reactivate KSHV from latency (Fig S2). Our work is the first to test
519 all four of the NICD isoforms in this capacity, and conclusively establishes that ectopic NICD2 is also
520 not capable of reactivating the virus. While ectopic expression of NICD isoforms 3 and 4 also did not
521 result in production of infectious virus, we are unable to conclude that NICD3 and 4 are similarly
522 insufficient to reactivate KSHV since we could not determine that they are transcriptionally active in our

523 experiments (Fig 7C). However, since the Notch isoforms have been shown to have different promoter
524 transactivation specificities (48, 82-84), it is possible that NICD3 and 4 are, in fact, active in Vero cells,
525 but are simply incapable of activating the 4x tandem RBP-Jk motif (4x CBS) reporter plasmid. NICD1
526 and 2 have been suggested to be functionally interchangeable in other biologic systems (85-87).

527 Despite Notch's inability to reactivate latent KSHV alone, we show that constitutive Notch1
528 activity is required for robust reactivation of the virus. All three of our strategies that inhibited
529 endogenous Notch activity in the Vero cells decreased Rta or VPA-induced reactivation over a range of
530 60-90% (Figs 2 to 4 and 6). Two of the strategies, DAPT treatment and dnMAML1 expression, are well-
531 established strategies to broadly inhibit all four Notch isoforms (2, 59, 61-65). DAPT blocks gamma-
532 secretase activation of endogenous Notch and dnMAML1 interferes with the formation of Notch
533 transactivation complexes (46, 88-90). However, neither strategy is strictly Notch-specific, because each
534 also interferes with other cellular processes that require gamma-secretase activity or cognate MAML1
535 (58, 60). To inhibit Notch1 specifically, we knocked-down its expression using two different transfected
536 siRNAs (Fig. 4). Inhibiting Notch with dnMAML1 reduced reactivation more dramatically than did
537 siRNA knock-down, suggesting that endogenous Notch 2, 3, and 4 may also have pro-viral functions
538 (compare Figs 3 and 4). Our Notch inhibition studies focused primarily on quantitating production of
539 infectious virus from latently infected Vero cells, but we also observed that inhibiting Notch in PEL
540 cells reduced synthesis of intracellular viral DNA (Fig 6A). Those data suggest that Notch activity in
541 both cell lines have similar effects on viral infection. We note a single contradictory study that
542 concluded that ectopic NICD1 reactivated KSHV (32).

543 It is well-established that Notch signaling is critical for cell and animal models of KSHV
544 pathogenesis; however, our data are the first to demonstrate that Notch activation is necessary for robust
545 production of infectious virus. Productive cycle gene expression is also seen in the context of sustained
546 Notch activation that is required for the endothelial to mesenchymal transition of KSHV-infected cells

547 (31, 35, 39, 40). Growth and survival of KSHV-infected cells also depend on Notch activity:
548 proliferation rates of KSHV-infected B cells were proportional to Notch expression levels, and Notch
549 inhibition reduced cellular cyclin D1 expression and arrested cells in G1 (37). Moreover, pharmacologic
550 Notch inhibition induced apoptosis of infected SLK, B, and primary KS tumor cells (31, 34, 35, 37-40)
551 and induced necrosis of PEL xenografts in NOD/SCID mice (36). Although Notch1 expression is
552 insufficient to productively reactivate KSHV, ectopic Notch1 could induce expression of a subset of
553 productive cycle viral genes in PEL cells (29). Importantly, the infected Vero cell model used in our
554 work is ideal for uncoupling the effect of Notch on cell growth from its effect on viral reactivation; in
555 our work, we used DAPT concentrations that significantly reduced production of infectious virus
556 without affecting host cell doubling time or survival (Fig 2E). This pro-viral role of Notch follows the
557 paradigm established in foundational tumor virus studies in which cellular oncogenic pathways
558 manipulated by SV40 or Adenovirus also support productive viral infections (91).
559 Our data raised two intriguing questions: how does activated Notch contribute to reactivation and
560 why is it not sufficient to reactivate KSHV alone? Since complete Notch ablation is inconsistent with
561 survival of KSHV-infected cells, one apparent contribution of activated Notch is to maintain survival of
562 cells in which KSHV is reactivating (31, 34, 36-40). To this end, we note that none of our strategies to
563 reduce Notch activity were 100% effective in debilitating virus production. However, our observation
564 that DAPT treatment and partial NICD1 knock-down can debilitate reactivation without reducing cell
565 growth suggests a function of Notch that is complementary to Rta and independent of cell survival.
566 Our data also show that NICD1 is transactivation competent in latently-infected Vero cells (Fig
567 7C), as has also been demonstrated in latently-infected PEL cells (29). Thus, all of the components
568 sufficient to form the Notch1 transactivation complex must be expressed and functional in KSHV-
569 infected cells (reviewed in (2, 3, 92)). Therefore, we believe that Notch's insufficiency to reactivate
570 KSHV derives from a limit to gene-specific transactivation that is relieved when Rta is expressed.

571 Importantly, one critical gene which ectopic NICD1 fails to activate in Vero and PEL cells is Rta (J.
572 DeCotiis-Mauro and D.M. Lukac, unpublished data (29)). Therefore, when endogenous Rta is induced
573 by VPA, or Rta is expressed ectopically, endogenous NICD1 then likely transactivates specific viral
574 genes during reactivation. Indeed, Notch forms complexes with vDNA in the presumptive promoters of
575 five viral genes (Fig 5), and Notch inhibition is associated with reduction in expression of four of the
576 genes and others not tested (Figs 2 and 3). Importantly, of the NICD1 targets identified herein,
577 ORF8/gB, ORF34, K8.1, ORF57/Mta, K8/KbZIP, and ORF59 are all essential for viral production in at
578 least one cell type (93-100). Our observation that broad Notch inhibitors have greater anti-viral potency
579 than specific Notch1 inhibition (compare Figs 2A and 3A to Fig 4A) suggests that at least one additional
580 Notch isoform also supports optimal KSHV reactivation.

581 We interpret our data as revealing that Notch activity had no influence on productive reactivation
582 unless Rta was expressed. Activated Notch has no intrinsic DNA binding ability, but instead relies upon
583 the cellular DNA binding protein RBP-Jk to specify NICD1's target genes (2, 3, 101) . One function of
584 Rta which can profoundly influence the ability of NICD1 to transactivate specific genes is Rta's ability
585 to stimulate RBP-Jk DNA binding (6, 9, 28). Our lab modeled this mechanism by showing that NICD1
586 can transactivate the Mta promoter only if a truncated form of Rta, lacking its transactivation domain,
587 stimulates RBP-Jk binding to the promoter (6). Studying the intact virus, we showed that KSHV
588 reactivation is associated with dramatic re-localization of RBP-Jk to unique sites on the virus genome
589 (28). The extent of dynamic RBP-Jk binding to the virus can be contrasted with that observed on the cell
590 genome. In uninfected cells, RBP-Jk binding sites on the cellular genome are classified as static or
591 dynamic, and NICD1 can stimulate RBP-Jk DNA binding to cellular genomes (102-105). However, on
592 the KSHV genome, the proportion of dynamic RBP-Jk sites in our studies vastly exceed the proportion
593 of dynamic sites reported on cellular genomes (28, 102, 103, 106-109). In fact, the number of
594 reactivation-specific RBP-Jk sites on the virus, and the number of RBP-Jk DNA motifs on the virus,

595 exceed the number of KSHV ORFs (28). Moreover, Rta is not found bound to the virus at every RBP-
596 Jk site (28). We hypothesize that NICD1/MAML1/RBP-Jk complexes transactivate specific essential
597 viral promoters and cooperate with Rta to support KSHV reactivation (Fig 8). During latency, in the
598 absence of Rta expression, NICD1/RBP-Jk fails to form a competent transactivation complex on at least
599 one essential viral promoter. Unlike NICD1, Rta also binds DNA independent of RBP-Jk for
600 transactivation and replication (110-113); these mechanistic differences probably also contribute to
601 Notch's insufficiency in reactivation.

602 Based on experimental data, we have published two mechanisms that describe how Rta regulates
603 RBP-Jk DNA binding: (1) Rta directly binds to RBP-Jk, and (2) Rta induces expression of additional
604 cellular proteins during reactivation which in turn bind to DNA adjacent to RBP-Jk (6, 9, 27, 28). The
605 latter mechanism is consistent with our work and others that demonstrated that *de novo* gene expression
606 downstream of Rta is required for robust reactivation (5, 27). Thus, NICD1 transactivation in KSHV-
607 infected cells is determined by the fate of the infection (latent vs. reactivating) and intracellular context,
608 as well as the DNA context of individual RBP-Jk binding sites. Similar context-dependent determinants
609 have been invoked to explain cell-specific variations in NICD1 transactivation and phenotypic
610 consequences in uninfected cells (48, 73-78, 109, 114-117). The influence of cellular context on Notch
611 function includes interactions between the four Notch isoforms, including competition, cooperation, or
612 redundancy (83, 85, 86, 118-131).

613 In Notch cancer biology, cell context is a major determinant of the striking observation that
614 Notch can be either tumor suppressive or oncogenic in different malignancies (reviewed in (2, 80, 132,
615 133)). The ideal DNA context for an NICD1-responsive RBP-Jk site is a head-to-head configuration
616 with a second RBP-Jk site spaced 15-17 nts apart (69-72); remarkably, only six pairs of RBP-Jk motifs
617 in the KSHV genome are found in that DNA context (J. DeCotiis-Mauro and D.M. Lukac, unpublished
618 data). It is likely that the mechanisms underlying contextual variations in Notch signaling outcomes in

619 uninfected cells are functionally similar in KSHV infection, but uniquely regulated by KSHV proteins
620 like Rta. Moreover, cell context may be responsible for the discordance of our observations with a
621 publication that showed that NICD1 inhibits KSHV reactivation in SLK cells (33).

622 In summary, herein we demonstrate the significance of constitutive Notch1 activity in the
623 cellular context of productive KSHV reactivation. The essentiality of Rta/RBP-Jk/DNA complexes in
624 driving reactivation is well-established, but this current study demonstrates that Notch contributes to
625 reactivation by forming promoter-specific NICD1/RBP-Jk/DNA complexes, also. The KSHV genome
626 contains >100 RBP-Jk motifs of varying sequence found in varying DNA contexts that we expect to
627 respond differently to Rta and/or NICD1 to determine the success of a reactivation signal leading to
628 virus production. Moreover, our data indicate that Notch isoforms other than the well-studied Notch1
629 may help regulate viral infection. This diversity in the molecular players underlies the consequences of
630 RBP-Jk-dependent gene expression in KSHV infection and host cell pathology. Our data are consistent
631 with the idea that the Notch-dependance of viral reactivation is a complex network that, when revealed,
632 will provide important new insights into Notch-dependent signaling in mammalian cells.

633

634 **Acknowledgements**

635 We gratefully thank Drs. Tom Kadesch, Jeff Vieira, Ethel Cesarman, Signe V. Horn Pederson, Geoff
636 Wahl, Rhett Kovall, Raphael Kopan, Jon C. Aster, and Spyros Artavanis-Tsakonas for cells, antibody,
637 and plasmids. The work was supported by NIH Grants AI117127 and AI150230.

638

639 **References**

640 1. Watanabe T, Sugimoto A, Hosokawa K, Fujimuro M. 2018. Signal Transduction Pathways
641 Associated with KSHV-Related Tumors. Adv Exp Med Biol 1045:321-355.
642 2. Aster JC, Pear WS, Blacklow SC. 2017. The Varied Roles of Notch in Cancer. Annu Rev Pathol
643 12:245-275.
644 3. Giaimo BD, Gagliani EK, Kovall RA, Borggrefe T. 2021. Transcription Factor RBPJ as a
645 Molecular Switch in Regulating the Notch Response, p 9-30. *In* Reichrath J, Reichrath S (ed),

646 Notch Signaling in Embryology and Cancer: Notch Signaling in Cancer doi:10.1007/978-3-030-
647 55031-8_2. Springer International Publishing, Cham.
648 4. Campbell M, Watanabe T, Nakano K, Davis RR, Lyu Y, Tepper CG, Durbin-Johnson B, Fujimuro
649 M, Izumiya Y. 2018. KSHV episomes reveal dynamic chromatin loop formation with domain-
650 specific gene regulation. Nat Commun 9:49.
651 5. Papp B, Motlagh N, Smindak RJ, Jin Jang S, Sharma A, Alonso JD, Toth Z. 2019. Genome-Wide
652 Identification of Direct RTA Targets Reveals Key Host Factors for Kaposi's Sarcoma-Associated
653 Herpesvirus Lytic Reactivation. J Virol 93.
654 6. Carroll KD, Bu W, Palmeri D, Spadavecchia S, Lynch SJ, Marras SA, Tyagi S, Lukac DM. 2006.
655 Kaposi's Sarcoma-associated herpesvirus lytic switch protein stimulates DNA binding of RBP-
656 Jk/CSL to activate the Notch pathway. J Virol 80:9697-709.
657 7. Liang Y, Chang J, Lynch S, Lukac DM, Ganem D. 2002. The lytic switch protein of KSHV
658 activates gene expression via functional interaction with RBP-Jk, the target of the Notch signaling
659 pathway. Genes Dev 16:1977-89.
660 8. Liang Y, Ganem D. 2003. Lytic but not latent infection by Kaposi's sarcoma-associated
661 herpesvirus requires host CSL protein, the mediator of Notch signaling. Proc Natl Acad Sci U S A
662 100:8490-5.
663 9. Palmeri D, Carroll KD, Gonzalez-Lopez O, Lukac DM. 2011. Kaposi's sarcoma-associated
664 herpesvirus Rta tetramers make high-affinity interactions with repetitive DNA elements in the Mta
665 promoter to stimulate DNA binding of RBP-Jk/CSL. J Virol 85:11901-15.
666 10. Hilton IB, Dittmer DP. 2012. Quantitative analysis of the bidirectional viral G-protein-coupled
667 receptor and lytic latency-associated nuclear antigen promoter of Kaposi's sarcoma-associated
668 herpesvirus. J Virol 86:9683-95.
669 11. Bu W, Carroll KD, Palmeri D, Lukac DM. 2007. The Kaposi's Sarcoma-associated
670 Herpesvirus/Human herpesvirus-8 ORF50/Rta Lytic Switch Protein Functions as a Tetramer. J
671 Virol 81:5788-5806.
672 12. Lukac D, Garibyan L, Kirshner J, Palmeri D, Ganem D. 2001. DNA binding by the Kaposi's
673 sarcoma-associated herpesvirus lytic switch protein is necessary for transcriptional activation of
674 two viral delayed early promoters. J Virol 75:6786-99.
675 13. Lukac DM, Kirshner JR, Ganem D. 1999. Transcriptional activation by the product of open
676 reading frame 50 of Kaposi's sarcoma-associated herpesvirus is required for lytic viral reactivation
677 in B cells. J Virol 73:9348-61.
678 14. Lukac DM, Renne R, Kirshner JR, Ganem D. 1998. Reactivation of Kaposi's sarcoma-associated
679 herpesvirus infection from latency by expression of the ORF 50 transactivator, a homolog of the
680 EBV R protein. Virology 252:304-312.
681 15. Wang Y, Yuan Y. 2006. Essential role of RBP-Jkappa in activation of the K8 delayed-early
682 promoter of Kaposi's sarcoma-associated herpesvirus by ORF50/RTA. Virology.
683 16. Persson LM, Wilson AC. 2010. Wide-scale use of Notch signaling factor CSL/RBP-Jkappa in
684 RTA-mediated activation of Kaposi's sarcoma-associated herpesvirus lytic genes. J Virol 84:1334-
685 47.
686 17. Scholz BA, Harth-Hertle ML, Malterer G, Haas J, Ellwart J, Schulz TF, Kempkes B. 2013.
687 Abortive lytic reactivation of KSHV in CBF1/CSL deficient human B cell lines. PLoS Pathog
688 9:e1003336.
689 18. Lan K, Kuppers DA, Verma SC, Robertson ES. 2004. Kaposi's sarcoma-associated herpesvirus-
690 encoded latency-associated nuclear antigen inhibits lytic replication by targeting Rta: a potential
691 mechanism for virus-mediated control of latency. J Virol 78:6585-94.

692 19. Liu Y, Cao Y, Liang D, Gao Y, Xia T, Robertson ES, Lan K. 2008. Kaposi's sarcoma-associated
693 herpesvirus RTA activates the processivity factor ORF59 through interaction with RBP-Jkappa
694 and a cis-acting RTA responsive element. Virology 380:264-75.
695 20. Liang Y, Ganem D. 2004. RBP-J (CSL) is essential for activation of the K14/vGPCR promoter of
696 Kaposi's sarcoma-associated herpesvirus by the lytic switch protein RTA. J Virol 78:6818-26.
697 21. Chang PJ, Boonsiri J, Wang SS, Chen LY, Miller G. 2010. Binding of RBP-Jkappa (CSL) protein
698 to the promoter of the Kaposi's sarcoma-associated herpesvirus ORF47 (gL) gene is a critical but
699 not sufficient determinant of transactivation by ORF50 protein. Virology 398:38-48.
700 22. Izumiya Y, Izumiya C, Hsia D, Ellison TJ, Luciw PA, Kung HJ. 2009. NF-kappaB serves as a
701 cellular sensor of Kaposi's sarcoma-associated herpesvirus latency and negatively regulates K-Rta
702 by antagonizing the RBP-Jkappa coactivator. J Virol 83:4435-46.
703 23. Sun R, LIn SF, Gradoville L, Yuan Y, Zhu F, Miller G. 1998. A viral gene that activates lytic cycle
704 expression of Kaposi's sarcoma-associated herpesvirus. Proc Natl Acad Sci USA 95:10866-10871.
705 24. Gradoville L, Gerlach J, Grogan E, Shedd D, Nikiforow S, Metroka C, Miller G. 2000. Kaposi's
706 sarcoma-associated herpesvirus open reading frame 50/Rta protein activates the entire lytic cycle
707 in the HH-B2 primary effusion lymphoma cell line. J Virol 74:6207-6212.
708 25. Nakamura H, Lu M, Gwack Y, Souvlis J, Zeichner SL, Jung JU. 2003. Global changes in Kaposi's
709 sarcoma-associated virus gene expression patterns following expression of a tetracycline-inducible
710 Rta transactivator. J Virol 77:4205-20.
711 26. Xu Y, AuCoin DP, Huete AR, Cei SA, Hanson LJ, Pari GS. 2005. A Kaposi's sarcoma-associated
712 herpesvirus/human herpesvirus 8 ORF50 deletion mutant is defective for reactivation of latent
713 virus and DNA replication. J Virol 79:3479-87.
714 27. Bu W, Palmeri D, Krishnan R, Marin R, Aris VM, Soteropoulous P, Lukac DM. 2008.
715 Identification of Direct Transcriptional Targets of the KSHV Rta Lytic Switch Protein by
716 conditional nuclear localization. J Virol 82:10709-10723.
717 28. Gonzalez-Lopez O DJ, Goyeneche C, Mello H, Vicente-Ortiz BA, Shin HJ, Driscoll KE, Du P,
718 Palmeri D, Lukac DM. . 2019. A herpesvirus transactivator and cellular POU proteins extensively
719 regulate DNA binding of the host Notch signaling protein RBP-Jκ to the virus genome. . J Biol
720 Chem 294:13073-13092.
721 29. Chang H, Dittmer DP, Chul SY, Hong Y, Jung JU. 2005. Role of Notch signal transduction in
722 Kaposi's sarcoma-associated herpesvirus gene expression. J Virol 79:14371-82.
723 30. DeCotiis JL, Ortiz NC, Vega BA, Lukac DM. 2017. An easily transfectable cell line that produces
724 an infectious reporter virus for routine and robust quantitation of Kaposi's sarcoma-associated
725 herpesvirus reactivation. J Virol Methods 247:99-106.
726 31. Cheng F, Pekkonen P, Laurinavicius S, Sugiyama N, Henderson S, Gunther T, Rantanen V,
727 Kaivanto E, Aavikko M, Sarek G, Hautaniemi S, Biberfeld P, Aaltonen L, Grundhoff A, Boshoff
728 C, Alitalo K, Lehti K, Ojala PM. 2011. KSHV-initiated notch activation leads to membrane-type-
729 1 matrix metalloproteinase-dependent lymphatic endothelial-to-mesenchymal transition. Cell Host
730 Microbe 10:577-90.
731 32. Lan K, Murakami M, Choudhuri T, Kuppers DA, Robertson ES. 2006. Intracellular-activated
732 Notch1 can reactivate Kaposi's sarcoma-associated herpesvirus from latency. Virology 351:393-
733 403.
734 33. Li S, Hu H, He Z, Liang D, Sun R, Lan K. 2016. Fine-Tuning of the Kaposi's Sarcoma-Associated
735 Herpesvirus Life Cycle in Neighboring Cells through the RTA-JAG1-Notch Pathway. PLOS
736 Pathogens 12:e1005900.
737 34. Curry CL, Reed LL, Golde TE, Miele L, Nickoloff BJ, Foreman KE. 2005. Gamma secretase
738 inhibitor blocks Notch activation and induces apoptosis in Kaposi's sarcoma tumor cells.
739 Oncogene 24:6333-44.

740 35. Emuss V, Lagos D, Pizzey A, Gratrix F, Henderson SR, Boshoff C. 2009. KSHV manipulates
741 Notch signaling by DLL4 and JAG1 to alter cell cycle genes in lymphatic endothelia. PLoS Pathog
742 5:e1000616.
743 36. Lan K, Murakami M, Bajaj B, Kaul R, He Z, Gan R, Feldman M, Robertson ES. 2009. Inhibition
744 of KSHV-infected primary effusion lymphomas in NOD/SCID mice by gamma-secretase
745 inhibitor. Cancer Biol Ther 8:2136-43.
746 37. Lan K, Choudhuri T, Murakami M, Kuppers DA, Robertson ES. 2006. Intracellular activated
747 Notch1 is critical for proliferation of Kaposi's sarcoma-associated herpesvirus-associated B-
748 lymphoma cell lines in vitro. J Virol 80:6411-9.
749 38. Lan K, Verma SC, Murakami M, Bajaj B, Kaul R, Robertson ES. 2007. Kaposi's sarcoma
750 herpesvirus-encoded latency-associated nuclear antigen stabilizes intracellular activated Notch by
751 targeting the Sel10 protein. Proc Natl Acad Sci U S A 104:16287-92.
752 39. Liu R, Li X, Tulpule A, Zhou Y, Scehnet JS, Zhang S, Lee JS, Chaudhary PM, Jung J, Gill PS.
753 2010. KSHV-induced notch components render endothelial and mural cell characteristics and cell
754 survival. Blood 115:887-95.
755 40. Gasperini P, Espigol-Frigole G, McCormick PJ, Salvucci O, Maric D, Uldrick TS, Polizzotto MN,
756 Yarchoan R, Tosato G. 2012. Kaposi sarcoma herpesvirus promotes endothelial-to-mesenchymal
757 transition through Notch-dependent signaling. Cancer Res 72:1157-69.
758 41. Gould F, Harrison SM, Hewitt EW, Whitehouse A. 2009. Kaposi's Sarcoma-Associated
759 Herpesvirus RTA Promotes Degradation of the Hey1 Repressor Protein through the Ubiquitin
760 Proteasome Pathway. Journal of Virology 83:6727-6738.
761 42. Green MR, Sambrook J, Sambrook J. 2012. Molecular cloning : a laboratory manual, 4th ed. Cold
762 Spring Harbor Laboratory Press, Cold Spring Harbor, N.Y.
763 43. Lukac DM, Renne R, Kirshner JR, Ganem D. 1998. Reactivation of Kaposi's Sarcoma-Associated
764 Herpesvirus Infection from Latency by Expression of the ORF 50 Transactivator, a Homolog of
765 the EBV R Protein. Virology 252:304-312.
766 44. Horn S, Kobberup S, Jørgensen MC, Kalisz M, Klein T, Kageyama R, Gegg M, Lickert H, Lindner
767 J, Magnuson MA, Kong Y-Y, Serup P, Ahnfelt-Rønne J, Jensen JN. 2012. Mind bomb
768 1 is required for pancreatic β-cell formation. Proceedings of the National Academy of
769 Sciences 109:7356-7361.
770 45. Kanda T, Sullivan KF, Wahl GM. 1998. Histone-GFP fusion protein enables sensitive analysis of
771 chromosome dynamics in living mammalian cells. Curr Biol 8:377-85.
772 46. Saxena MT, Schroeter EH, Mumm JS, Kopan R. 2001. Murine Notch Homologs (N1–4)
773 Undergo Presenilin-dependent Proteolysis *. Journal of Biological Chemistry 276:40268-40273.
774 47. Yuan Z, Friedmann DR, VanderWielen BD, Collins KJ, Kovall RA. 2012. Characterization of
775 CSL (CBF-1, Su(H), Lag-1) mutants reveals differences in signaling mediated by Notch1 and
776 Notch2. J Biol Chem 287:34904-16.
777 48. Ong CT, Cheng HT, Chang LW, Ohtsuka T, Kageyama R, Stormo GD, Kopan R. 2006. Target
778 selectivity of vertebrate notch proteins. Collaboration between discrete domains and CSL-binding
779 site architecture determines activation probability. J Biol Chem 281:5106-19.
780 49. Weng AP, Ferrando AA, Lee W, Morris JPt, Silverman LB, Sanchez-Irizarry C, Blacklow SC,
781 Look AT, Aster JC. 2004. Activating mutations of NOTCH1 in human T cell acute lymphoblastic
782 leukemia. Science 306:269-71.
783 50. Gantt S, Carlsson J, Ikoma M, Gachelet E, Gray M, Geballe AP, Corey L, Casper C, Lagunoff M,
784 Vieira J. 2011. The HIV protease inhibitor nelfinavir inhibits Kaposi's sarcoma-associated
785 herpesvirus replication in vitro. Antimicrobial agents and chemotherapy 55:2696-703.
786 51. Carroll KD, Khadim F, Spadavecchia S, Palmeri D, Lukac DM. 2007. Direct interactions of
787 Kaposi's sarcoma-associated herpesvirus/human herpesvirus 8 ORF50/Rta protein with the

788 cellular protein octamer-1 and DNA are critical for specifying transactivation of a delayed-early
789 promoter and stimulating viral reactivation. J Virol 81:8451-67.
790 52. Kirshner JR, Lukac DM, Chang J, Ganem D. 2000. Kaposi's Sarcoma-Associated Herpesvirus
791 Open Reading Frame 57 Encodes a Posttranscriptional Regulator with Multiple Distinct Activities.
792 J Virol 74:3586-3597.
793 53. Bruce AG, Barcy S, DiMaio T, Gan E, Garrigues HJ, Lagunoff M, Rose TM. 2017. Quantitative
794 Analysis of the KSHV Transcriptome Following Primary Infection of Blood and Lymphatic
795 Endothelial Cells. Pathogens 6.
796 54. Journo G, Tushinsky C, Shterngas A, Avital N, Eran Y, Karpuj MV, Frenkel-Morgenstern M,
797 Shamay M. 2018. Modulation of Cellular CpG DNA Methylation by Kaposi's Sarcoma-Associated
798 Herpesvirus. J Virol 92.
799 55. Gonzalez-Lopez O, Goyeneche, C, DeCotiis, J Vicente-Ortiz, BA, Shin H, Driscoll, K, Du P,
800 Palmeri, D, and DM Lukac. 2019. Viral Rta and cellular POU proteins regulate dynamic, genome-
801 wide DNA binding of the Notch pathway protein Recombination Signal Binding Protein (RBP)-
802 Jk during reactivation of Kaposi's sarcoma-associated herpesvirus (KSHV). Submitted.
803 56. Nelson JD, Denisenko O, Bomsztyk K. 2006. Protocol for the fast chromatin immunoprecipitation
804 (ChIP) method. Nature Protocols 1:179-185.
805 57. Ross S. 2003. Peirce's criterion for the elimination of suspect experimental data. J Eng Technol
806 20.
807 58. Güner G, Lichtenthaler SF. 2020. The substrate repertoire of γ-secretase/presenilin. Seminars in
808 Cell & Developmental Biology 105:27-42.
809 59. Weng AP, Nam Y, Wolfe MS, Pear WS, Griffin JD, Blacklow SC, Aster JC. 2003. Growth
810 Suppression of Pre-T Acute Lymphoblastic Leukemia Cells by Inhibition of Notch Signaling.
811 Molecular and Cellular Biology 23:655-664.
812 60. Zema S, Pelullo M, Nardozza F, Felli MP, Screpanti I, Bellavia D. 2020. A Dynamic Role of
813 Mastermind-Like 1: A Journey Through the Main (Path)ways Between Development and Cancer.
814 Frontiers in Cell and Developmental Biology 8.
815 61. Maillard I, Weng AP, Carpenter AC, Rodriguez CG, Sai H, Xu L, Allman D, Aster JC, Pear WS.
816 2004. Mastermind critically regulates Notch-mediated lymphoid cell fate decisions. Blood
817 104:1696-1702.
818 62. Saravanamuthu SS, Gao CY, Zelenka PS. 2009. Notch signaling is required for lateral induction
819 of Jagged1 during FGF-induced lens fiber differentiation. Dev Biol 332:166-76.
820 63. Bagheri L, Pellati A, Rizzo P, Aquila G, Massari L, De Mattei M, Ongaro A. 2018. Notch pathway
821 is active during osteogenic differentiation of human bone marrow mesenchymal stem cells induced
822 by pulsed electromagnetic fields. J Tissue Eng Regen Med 12:304-315.
823 64. Lilly B, Kennard S. 2009. Differential gene expression in a coculture model of angiogenesis
824 reveals modulation of select pathways and a role for Notch signaling. Physiol Genomics 36:69-78.
825 65. Sastre M, Steiner H, Fuchs K, Capell A, Multhaup G, Condron MM, Teplow DB, Haass C. 2001.
826 Presenilin-dependent γ-secretase processing of β-amyloid precursor protein at a site corresponding
827 to the S3 cleavage of Notch. EMBO reports 2:835-841.
828 66. Shin HJ, Decotiis J, Giron M, Palmeri D, Lukac DM. 2014. Histone Deacetylase Classes I and II
829 Regulate Kaposi's Sarcoma-Associated Herpesvirus Reactivation. J Virol 88:1281-92.
830 67. You W-K, Schuetz TJ, Lee SH. 2023. Targeting the DLL/Notch Signaling Pathway in Cancer:
831 Challenges and Advances in Clinical Development. Molecular Cancer Therapeutics 22:3-11.
832 68. Hori K, Sen A, Artavanis-Tsakonas S. 2013. Notch signaling at a glance. J Cell Sci 126:2135-40.
833 69. Nam Y, Sliz P, Pear WS, Aster JC, Blacklow SC. 2007. Cooperative assembly of higher-order
834 Notch complexes functions as a switch to induce transcription. Proc Natl Acad Sci U S A
835 104:2103-8.

836 70. Nam Y, Sliz P, Song L, Aster JC, Blacklow SC. 2006. Structural basis for cooperativity in
837 recruitment of MAML coactivators to Notch transcription complexes. Cell 124:973-83.
838 71. Arnett KL, Hass M, McArthur DG, Ilagan MX, Aster JC, Kopan R, Blacklow SC. 2010. Structural
839 and mechanistic insights into cooperative assembly of dimeric Notch transcription complexes. Nat
840 Struct Mol Biol 17:1312-7.
841 72. Liu H, Chi AW, Arnett KL, Chiang MY, Xu L, Shestova O, Wang H, Li YM, Bhandoola A, Aster
842 JC, Blacklow SC, Pear WS. 2010. Notch dimerization is required for leukemogenesis and T-cell
843 development. Genes Dev 24:2395-407.
844 73. Castro B, Barolo S, Bailey AM, Posakony JW. 2005. Lateral inhibition in proneural clusters: cis-
845 regulatory logic and default repression by Suppressor of Hairless. Development 132:3333-3344.
846 74. Nellesen DT, Lai EC, Posakony JW. 1999. Discrete enhancer elements mediate selective
847 responsiveness of enhancer of split complex genes to common transcriptional activators. Dev Biol
848 213:33-53.
849 75. Wang H, Zou J, Zhao B, Johannsen E, Ashworth T, Wong H, Pear WS, Schug J, Blacklow SC,
850 Arnett KL, Bernstein BE, Kieff E, Aster JC. 2011. Genome-wide analysis reveals conserved and
851 divergent features of Notch1/RBPJ binding in human and murine T-lymphoblastic leukemia cells.
852 Proc Natl Acad Sci U S A 108:14908-13.
853 76. Swanson CI, Evans NC, Barolo S. 2010. Structural rules and complex regulatory circuitry
854 constrain expression of a Notch- and EGFR-regulated eye enhancer. Dev Cell 18:359-70.
855 77. Cave JW, Loh F, Surpris JW, Xia L, Caudy MA. 2005. A DNA transcription code for cell-specific
856 gene activation by notch signaling. Curr Biol 15:94-104.
857 78. Basak O, Giachino C, Fiorini E, MacDonald HR, Taylor V. 2012. Neurogenic Subventricular Zone
858 Stem/Progenitor Cells Are Notch1-Dependent in Their Active But Not Quiescent State. The
859 Journal of Neuroscience 32:5654-5666.
860 79. Bray SJ. 2016. Notch signalling in context. Nature Reviews Molecular Cell Biology 17:722-735.
861 80. Arruga F, Vaisitti T, Deaglio S. 2018. The NOTCH Pathway and Its Mutations in Mature B Cell
862 Malignancies. Frontiers in Oncology 8.
863 81. Chiang MY, Xu L, Shestova O, Histen G, L'Heureux S, Romany C, Childs ME, Gimotty PA, Aster
864 JC, Pear WS. 2008. Leukemia-associated NOTCH1 alleles are weak tumor initiators but accelerate
865 K-ras-initiated leukemia. J Clin Invest 118:3181-94.
866 82. Beatus P, Lundkvist J, Oberg C, Pedersen K, Lendahl U. 2001. The origin of the ankyrin repeat
867 region in Notch intracellular domains is critical for regulation of HES promoter activity. Mech
868 Dev 104:3-20.
869 83. James AC, Szot JO, Iyer K, Major JA, Pursglove SE, Chapman G, Dunwoodie SL. 2014. Notch4
870 reveals a novel mechanism regulating Notch signal transduction. Biochim Biophys Acta
871 1843:1272-84.
872 84. Yamaguchi N, Oyama T, Ito E, Satoh H, Azuma S, Hayashi M, Shimizu K, Honma R, Yanagisawa
873 Y, Nishikawa A, Kawamura M, Imai J-i, Ohwada S, Tatsuta K, Inoue J-i, Semba K, Watanabe S.
874 2008. NOTCH3 Signaling Pathway Plays Crucial Roles in the Proliferation of ErbB2-Negative
875 Human Breast Cancer Cells. Cancer Research 68:1881-1888.
876 85. Liu Z, Brunskill E, Varnum-Finney B, Zhang C, Zhang A, Jay PY, Bernstein I, Morimoto M,
877 Kopan R. 2015. The intracellular domains of Notch1 and Notch2 are functionally equivalent
878 during development and carcinogenesis. Development 142:2452-2463.
879 86. Giachino C, Boulay JL, Ivanek R, Alvarado A, Tostado C, Lugert S, Tchorz J, Coban M, Mariani
880 L, Bettler B, Lathia J, Frank S, Pfister S, Kool M, Taylor V. 2015. A Tumor Suppressor Function
881 for Notch Signaling in Forebrain Tumor Subtypes. Cancer Cell 28:730-742.
882 87. Rossi D, Trifonov V, Fangazio M, Bruscaggin A, Rasi S, Spina V, Monti S, Vaisitti T, Arruga F,
883 Famà R, Ciardullo C, Greco M, Cresta S, Piranda D, Holmes A, Fabbri G, Messina M, Rinaldi A,

884 Wang J, Agostinelli C, Piccaluga PP, Lucioni M, Tabbò F, Serra R, Franceschetti S, Deambrogi
885 C, Daniele G, Gattei V, Marasca R, Facchetti F, Arcaini L, Inghirami G, Bertoni F, Pileri SA,
886 Deaglio S, Foà R, Dalla-Favera R, Pasqualucci L, Rabadan R, Gaidano G. 2012. The coding
887 genome of splenic marginal zone lymphoma: activation of NOTCH2 and other pathways
888 regulating marginal zone development. Journal of Experimental Medicine 209:1537-1551.
889 88. De Strooper B, Annaert W, Cupers P, Saftig P, Craessaerts K, Mumm JS, Schroeter EH, Schrijvers
890 V, Wolfe MS, Ray WJ, Goate A, Kopan R. 1999. A presenilin-1-dependent γ-secretase-like
891 protease mediates release of Notch intracellular domain. Nature 398:518-522.
892 89. Lin SE, Oyama T, Nagase T, Harigaya K, Kitagawa M. 2002. Identification of new human
893 mastermind proteins defines a family that consists of positive regulators for notch signaling. J Biol
894 Chem 277:50612-20.
895 90. Wu L, Sun T, Kobayashi K, Gao P, Griffin JD. 2002. Identification of a family of mastermind-like
896 transcriptional coactivators for mammalian notch receptors. Mol Cell Biol 22:7688-700.
897 91. DiMaio D. 2019. Small size, big impact: how studies of small DNA tumour viruses revolutionized
898 biology. Philos Trans R Soc Lond B Biol Sci 374:20180300.
899 92. Siebel C, Lendahl U. 2017. Notch Signaling in Development, Tissue Homeostasis, and Disease.
900 Physiol Rev 97:1235-1294.
901 93. Zhou Y, Tian X, Wang S, Gao M, Zhang C, Ma J, Cheng X, Bai L, Qin HB, Luo MH, Qin Q,
902 Jiang B, Lan K, Zhang J. 2024. Palmitoylation of KSHV pORF55 is required for Golgi localization
903 and efficient progeny virion production. PLoS Pathog 20:e1012141.
904 94. Dollery SJ, Santiago-Crespo RJ, Chatterjee D, Berger EA. 2019. Glycoprotein K8.1A of Kaposi's
905 Sarcoma-Associated Herpesvirus Is a Critical B Cell Tropism Determinant Independent of Its
906 Heparan Sulfate Binding Activity. J Virol 93.
907 95. Han Z, Swaminathan S. 2006. Kaposi's sarcoma-associated herpesvirus lytic gene ORF57 is
908 essential for infectious virion production. J Virol 80:5251-60.
909 96. Majerciak V, Pripuzova N, McCoy JP, Gao SJ, Zheng ZM. 2007. Targeted disruption of Kaposi's
910 sarcoma-associated herpesvirus ORF57 in the viral genome is detrimental for the expression of
911 ORF59, K8alpha, and K8.1 and the production of infectious virus. J Virol 81:1062-71.
912 97. Wang Y, Sathish N, Hollow C, Yuan Y. 2011. Functional characterization of Kaposi's sarcoma-
913 associated herpesvirus open reading frame K8 by bacterial artificial chromosome-based
914 mutagenesis. J Virol 85:1943-57.
915 98. Krishnan HH, Sharma-Walia N, Zeng L, Gao SJ, Chandran B. 2005. Envelope glycoprotein gB of
916 Kaposi's sarcoma-associated herpesvirus is essential for egress from infected cells. J Virol
917 79:10952-67.
918 99. Nishimura M, Watanabe T, Yagi S, Yamanaka T, Fujimuro M. 2017. Kaposi's sarcoma-associated
919 herpesvirus ORF34 is essential for late gene expression and virus production. Sci Rep 7:329.
920 100. Peng C, Chen J, Tang W, Liu C, Chen X. 2014. Kaposi's sarcoma-associated herpesvirus ORF6
921 gene is essential in viral lytic replication. PLoS One 9:e99542.
922 101. Sprinzak D, Blacklow SC. 2021. Biophysics of Notch Signaling. Annu Rev Biophys 50:157-189.
923 102. Wang H, Zang C, Taing L, Arnett KL, Wong YJ, Pear WS, Blacklow SC, Liu XS, Aster JC. 2014.
924 NOTCH1-RBPJ complexes drive target gene expression through dynamic interactions with
925 superenhancers. Proc Natl Acad Sci U S A 111:705-10.
926 103. Castel D, Mourikis P, Bartels SJ, Brinkman AB, Tajbakhsh S, Stunnenberg HG. 2013. Dynamic
927 binding of RBPJ is determined by Notch signaling status. Genes Dev 27:1059-71.
928 104. Krejci A, Bray S. 2007. Notch activation stimulates transient and selective binding of Su(H)/CSL
929 to target enhancers. Genes Dev 21:1322-7.
930 105. Gomez-Lamarca MJ, Falo-Sanjuan J, Stojnic R, Abdul Rehman S, Muresan L, Jones ML, Pillidge
931 Z, Cerda-Moya G, Yuan Z, Baloul S, Valenti P, Bystricky K, Payre F, O'Holleran K, Kovall R,

932 Bray SJ. 2018. Activation of the Notch Signaling Pathway In Vivo Elicits Changes in CSL Nuclear
933 Dynamics. Developmental Cell 44:611-623.e7.
934 106. Zhao B, Zou J, Wang H, Johannsen E, Peng CW, Quackenbush J, Mar JC, Morton CC, Freedman
935 ML, Blacklow SC, Aster JC, Bernstein BE, Kieff E. 2011. Epstein-Barr virus exploits intrinsic B-
936 lymphocyte transcription programs to achieve immortal cell growth. Proc Natl Acad Sci U S A
937 108:14902-7.
938 107. Severson E, Arnett KL, Wang H, Zang C, Taing L, Liu H, Pear WS, Shirley Liu X, Blacklow SC,
939 Aster JC. 2017. Genome-wide identification and characterization of Notch transcription complex–
940 binding sequence-paired sites in leukemia cells. Science Signaling 10:eaag1598.
941 108. Ryan RJH, Petrovic J, Rausch DM, Zhou Y, Lareau CA, Kluk MJ, Christie AL, Lee WY, Tarjan
942 DR, Guo B, Donohue LKH, Gillespie SM, Nardi V, Hochberg EP, Blacklow SC, Weinstock DM,
943 Faryabi RB, Bernstein BE, Aster JC, Pear WS. 2017. A B Cell Regulome Links Notch to
944 Downstream Oncogenic Pathways in Small B Cell Lymphomas. Cell Reports 21:784-797.
945 109. Yashiro-Ohtani Y, Wang H, Zang C, Arnett KL, Bailis W, Ho Y, Knoechel B, Lanauze C, Louis
946 L, Forsyth KS, Chen S, Chung Y, Schug J, Blobel GA, Liebhaber SA, Bernstein BE, Blacklow
947 SC, Liu XS, Aster JC, Pear WS. 2014. Long-range enhancer activity determines Myc
948 sensitivity to Notch inhibitors in T cell leukemia. Proceedings of the National Academy of
949 Sciences doi:10.1073/pnas.1407079111:201407079.
950 110. Song M, Brown H, Wu T-T, Sun R. 2001. Transcription activation of polyadenylated nuclear RNA
951 by Rta in Human herpesvirus 8/Kaposi's Sarcoma-associated herpesvirus. J Virol 75:3129-40.
952 111. Chen J, Ye F, Xie J, Kuhne K, Gao SJ. 2009. Genome-wide identification of binding sites for
953 Kaposi's sarcoma-associated herpesvirus lytic switch protein, RTA. Virology 386:290-302.
954 112. Wang Y, Li H, Chan MY, Zhu FX, Lukac DM, Yuan Y. 2004. Kaposi's sarcoma-associated
955 herpesvirus ori-Lyt-dependent DNA replication: cis-acting requirements for replication and ori-
956 Lyt-associated RNA transcription. J Virol 78:8615-29.
957 113. Rossetto CC, Susilarini NK, Pari GS. 2011. Interaction of Kaposi's sarcoma-associated herpesvirus
958 ORF59 with oriLyt is dependent on binding with K-Rta. J Virol 85:3833-41.
959 114. Cooper MT, Tyler DM, Furriols M, Chalkiadaki A, Delidakis C, Bray S. 2000. Spatially restricted
960 factors cooperate with notch in the regulation of Enhancer of split genes. Dev Biol 221:390-403.
961 115. Takebayashi K, Sasai Y, Sakai Y, Watanabe T, Nakanishi S, Kageyama R. 1994. Structure,
962 chromosomal locus, and promoter analysis of the gene encoding the mouse helix-loop-helix factor
963 HES-1. Negative autoregulation through the multiple N box elements. J Biol Chem 269:5150-6.
964 116. Stoeck A, Lejnine S, Truong A, Pan L, Wang H, Zang C, Yuan J, Ware C, MacLean J, Garrett-
965 Engele PW, Kluk M, Laskey J, Haines BB, Moskaluk C, Zawel L, Fawell S, Gilliland G, Zhang
966 T, Kremer BE, Knoechel B, Bernstein BE, Pear WS, Liu XS, Aster JC, Sathyanarayanan S. 2014.
967 Discovery of biomarkers predictive of GSI response in triple-negative breast cancer and adenoid
968 cystic carcinoma. Cancer Discov 4:1154-67.
969 117. Krejcí A, Bernard F, Housden BE, Collins S, Bray SJ. 2009. Direct response to Notch activation:
970 signaling crosstalk and incoherent logic. Sci Signal 2:ra1.
971 118. Choi SH, Severson E, Pear WS, Liu XS, Aster JC, Blacklow SC. 2017. The common oncogenomic
972 program of NOTCH1 and NOTCH3 signaling in T-cell acute lymphoblastic leukemia. PLOS ONE
973 12:e0185762.
974 119. Bellavia D, Campese AF, Checquolo S, Balestri A, Biondi A, Cazzaniga G, Lendahl U, Fehling
975 HJ, Hayday AC, Frati L, von Boehmer H, Gulino A, Screpanti I. 2002. Combined expression of
976 pTα and Notch3 in T cell leukemia identifies the requirement of preTCR for leukemogenesis.
977 Proceedings of the National Academy of Sciences 99:3788-3793.

978 120. Engler A, Rolando C, Giachino C, Saotome I, Erni A, Brien C, Zhang R, Zimber-Strobl U, Radtke
979 F, Artavanis-Tsakonas S, Louvi A, Taylor V. 2018. Notch2 Signaling Maintains NSC Quiescence
980 in the Murine Ventricular-Subventricular Zone. Cell Reports 22:992-1002.
981 121. Meester JAN, Verstraeten A, Alaerts M, Schepers D, Van Laer L, Loeys BL. 2019. Overlapping
982 but distinct roles for NOTCH receptors in human cardiovascular disease. Clinical Genetics 95:85-
983 94.
984 122. Beatus P, Lundkvist J, Oberg C, Lendahl U. 1999. The notch 3 intracellular domain represses
985 notch 1-mediated activation through Hairy/Enhancer of split (HES) promoters. Development
986 126:3925-3935.
987 123. Beà S, Valdés-Mas R, Navarro A, Salaverria I, Martín-Garcia D, Jares P, Giné E, Pinyol M, Royo
988 C, Nadeu F, Conde L, Juan M, Clot G, Vizán P, Di Croce L, Puente DA, López-Guerra M, Moros
989 A, Roue G, Aymerich M, Villamor N, Colomo L, Martínez A, Valera A, Martín-Subero JI,
990 Amador V, Hernández L, Rozman M, Enjuanes A, Forcada P, Muntañola A, Hartmann EM,
991 Calasanz MJ, Rosenwald A, Ott G, Hernández-Rivas JM, Klapper W, Siebert R, Wiestner A,
992 Wilson WH, Colomer D, López-Guillermo A, López-Otín C, Puente XS, Campo E. 2013.
993 Landscape of somatic mutations and clonal evolution in mantle cell lymphoma. Proceedings of the
994 National Academy of Sciences 110:18250-18255.
995 124. Ables JL, DeCarolis NA, Johnson MA, Rivera PD, Gao Z, Cooper DC, Radtke F, Hsieh J, Eisch
996 AJ. 2010. Notch1 Is Required for Maintenance of the Reservoir of Adult Hippocampal Stem Cells.
997 The Journal of Neuroscience 30:10484-10492.
998 125. Nwabo Kamdje AH, Bassi G, Pacelli L, Malpeli G, Amati E, Nichele I, Pizzolo G, Krampera M.
999 2012. Role of stromal cell-mediated Notch signaling in CLL resistance to chemotherapy. Blood
1000 Cancer Journal 2:e73-e73.
1001 126. Demehri S, Turkoz A, Manivasagam S, Yockey Laura J, Turkoz M, Kopan R. 2012. Elevated
1002 Epidermal Thymic Stromal Lymphopoietin Levels Establish an Antitumor Environment in the
1003 Skin. Cancer Cell 22:494-505.
1004 127. Boucher JM, Harrington A, Rostama B, Lindner V, Liaw L. 2013. A Receptor-Specific Function
1005 for Notch2 in Mediating Vascular Smooth Muscle Cell Growth Arrest Through Cyclin-dependent
1006 Kinase Inhibitor 1B. Circulation Research 113:975-985.
1007 128. Southgate L, Sukalo M, Karountzos ASV, Taylor EJ, Collinson CS, Ruddy D, Snape KM,
1008 Dallapiccola B, Tolmie JL, Joss S, Brancati F, Digilio MC, Graul-Neumann LM, Salviati L, Coerdt
1009 W, Jacquemin E, Wuyts W, Zenker M, Machado RD, Trembath RC. 2015. Haploinsufficiency of
1010 the NOTCH1 Receptor as a Cause of Adams–Oliver Syndrome With Variable Cardiac
1011 Anomalies. Circulation: Cardiovascular Genetics 8:572-581.
1012 129. Kawai H, Kawaguchi D, Kuebrich BD, Kitamoto T, Yamaguchi M, Gotoh Y, Furutachi S. 2017.
1013 Area-Specific Regulation of Quiescent Neural Stem Cells by Notch3 in the Adult Mouse
1014 Subependymal Zone. The Journal of Neuroscience 37:11867-11880.
1015 130. Arasada RR, Amann JM, Rahman MA, Huppert SS, Carbone DP. 2014. EGFR blockade enriches
1016 for lung cancer stem-like cells through Notch3-dependent signaling. Cancer Research
1017 doi:10.1158/0008-5472.Can-13-3724:canres.3724.2013.
1018 131. Kofler NM, Cuervo H, Uh MK, Murtomäki A, Kitajewski J. 2015. Combined deficiency of Notch1
1019 and Notch3 causes pericyte dysfunction, models CADASIL and results in arteriovenous
1020 malformations. Scientific Reports 5:16449.
1021 132. Parmigiani E, Taylor V, Giachino C. 2020. Oncogenic and Tumor-Suppressive Functions of
1022 NOTCH Signaling in Glioma. Cells 9:2304.
1023 133. D'Assoro AB, Leon-Ferre R, Braune EB, Lendahl U. 2022. Roles of Notch Signaling in the Tumor
1024 Microenvironment. Int J Mol Sci 23.

1025 134. Schneider CA, Rasband WS, Eliceiri KW. 2012. NIH Image to ImageJ: 25 years of image analysis.
1026 Nature Methods 9:671-675.

1027

1028

1029 **FIGURE LEGENDS**

1030 **Figure 1. Endogenous Notch1 is constitutively active in infected Vero cells. A.** Total cellular protein
1031 was harvested in RIPA buffer from triplicate cultures of 4 x 10^5 cells Vero rKSHV.294 cells, uninfected
1032 Vero cells, or uninfected Vero cells transfected plasmid expressing NICD1. Equal amounts of each extract
1033 were separated on a 4-12% PAGE gradient gel electrophoresed in Tris-MOPS-SDS buffer. Proteins
1034 transferred to nitrocellulose were probed with Notch1-specific bTAN20 antibody (1:500) or anti-GAPDH
1035 antibody (1:5000), followed by HRP-conjugated anti-rat secondary antibody (1:5000). Bands were
1036 visualized by ChemiDoc (BioRad). **B. Quantitation.** NICD1 and GAPD bands were measured by ImageJ
1037 (134). NICD1 values were divided by GAPDH values and plotted. *$p<0.002$ by t test.

1038
1039
1040 **Figure 2. Notch inhibition reduces Rta-mediated reactivation without inhibiting cell growth.**
1041
1042 **A. Treatment with a gamma secretase inhibitor decreases viral reactivation by Rta.** Vero
1043 rKSHV.294 cells were treated with 1 or 5 uM DAPT, or vehicle control ("Vh") 24h prior to transfection
1044 with 2.5 ug of Rta expression vector. At 72h post-transfection, infectious virus was quantitated by
1045 transferring the media to the 293 MSR tet-OFF complementing reporter cells as described in Methods.
1046 SeAP was measured in 25 uL of media per infection using the Phospha-Light System (Applied
1047 Biosystems). SeAP values from media alone were subtracted from each experimental value, and folds
1048 were calculated by normalizing to samples treated with vehicle and transfected with empty vector.
1049 *$p<0.05$ by t test compared to Vec + Vh.

1050 **B. Treatment with a gamma secretase inhibitor decreases activity of a Notch-dependent reporter**
1051 **plasmid.** Vero rKSHV.294 cells were transfected with Notch reporter plasmid pGL2-4xCSL expressing

1052 firefly luciferase ("Jk") and pcDNA3.1-HisLacZ expressing β-galactosidase ("Cont"). Cells were treated
1053 with 5 uM DAPT or vehicle (DMSO) 24hr post-transfection, and total cellular protein was extracted.
1054 Luciferase values were normalized to βgal values at each timepoint. *p<0.0015 and **p<0.0001 by t test
1055 compared to Cont at 6h and 24h.

1056 **C. and D. Expression of KSHV transcripts are reduced by inhibiting endogenous Notch1.**
1057 Triplicate cultures of Vero rKSHV.294 cells were transfected with empty vector or Rta expression
1058 vector and treated with vehicle or DAPT (5 uM DAPT), as in Fig 2A. Total RNA was harvested 24 h
1059 after transfection and transcripts for the indicated viral genes were quantitated by real-time quantitative
1060 reverse-transcription/PCR. Transcription of the indicated viral genes was calculated by the delta-delta Ct
1061 method using cellular beta-actin transcription as the internal control for each sample and Vec + vehicle
1062 as baseline fold. One outlying value per transfection was removed using Peirce's method. *p<0.05 by t
1063 test comparing Rta + vehicle (DMSO) to Rta + 5 uM DAPT**.** Each primer pair was also tested without
1064 adding reverse transcriptase to the input RNA and no amplicons were detected (D.M. Lukac,
1065 unpublished data).
1066 **E. Notch inhibition by DAPT treatment does not affect Vero rKSHV.294 cell growth.** Triplicate
1067 cultures of Vero rKSHV.294 cells were treated in two biologic replicates with vehicle or DAPT at the
1068 indicated concentrations as described in Fig 2A. At the post-treatment times indicated, cell viability was
1069 quantitated using Alamar Blue (BioRad). Mock values were averaged and subtracted from each
1070 experimental value to yield corrected values. All corrected values were then normalized to 0h values
1071 that had been set to the relative value of 1 for each treatment. The slight enhancement of cell growth rate
1072 when compared to the vehicle control was not statistically-significant.

1073

1074 **Fig 3. Inhibition of endogenous Notch by dominant negative MAML1 mutants inhibit viral**
1075 **reactivation and expression of some viral genes. A.** Vero rKSHV.294 cells were transfected with 1ug

1076 of plasmids expressing Rta and two different dnMAML alleles ("dnMAM" "A" and "B"; each fused to
1077 GFP). Infectious virus was quantitated as in Fig. 2A. *p<0.02 and **p<0.01 by t test compared to Rta
1078 plus Vector. **B. dnMAML1 proteins are well-expressed in infected Vero rKSHV.294 cells.** Vero
1079 rKSHV.294 cells were transfected as in Fig 3A, total protein was harvested in RIPA buffer 48h later,
1080 Western blotted, and probed with GFP-specific antiserum to detect the dnMAML-GFP fusion proteins.
1081 As a control for the Western blot, plasmid expressing H2b-GFP was also transfected into cells ("H2b").
1082 Equivalent loading of lanes was verified by probing for endogenous histone H3 ("control").
1083 **C. Expression of KSHV proteins are reduced by inhibiting endogenous Notch1.** Expression of the
1084 KSHV proteins Mta, KbZIP, and ORF59 in extracts from cells transfected as in Fig 3B were visualized
1085 by Western blotting. Fold induction of each viral protein was determined by normalizing to expression
1086 of the host protein Histone H3 ("H3") in each lane, then dividing by the value for Vec alone, which had
1087 been set to "1." Those values are listed under each corresponding lane. **D. Quantitation**. The relative
1088 reduction of viral protein expression by inhibiting Notch1 was calculated by comparing each viral
1089 protein's induction by ectopic Rta + Vec with that induced by Rta in the presence of ectopic dnMAML1
1090 in panel B. Rta alone was set at 100. *p<0.09 and **p<0.005 by t test compared to Rta + Vec**.**
1091
1092 **Fig 4. Activated Notch1 is required for optimal reactivation of KSHV. A. Reactivation by ectopic**
1093 **Rta.** Vero rKSHV.294 cells were transfected with 30 pM of either scrambled siRNA (Scr; control),
1094 Notch 1 siRNA A (N1-A), or Notch 1 siRNA B (N1-B) in triplicate sets. 48h later, Rta expression
1095 vector or Vec (as control) was transfected into each of the siRNA-transfected cells. 48h post-
1096 transfection, virus containing media were transferred to 293 MSR tet-OFF cells. Infectious virus was
1097 quantitated as in Fig. 2A. *p<0.02 by t test compared to Rta + Scr **. B. Reactivation by VPA treatment.**
1098 Vero rKSHV.294 cells were transfected with 30pM of either scrambled siRNA (Scr; control) or Notch 1
1099 siRNA B (N1-B). 54h later, 1 mM VPA was added to the siRNA-transfected cells. 72h post-
1100 transfection, virus containing media were transferred to 293 MSR tet-OFF cells. Infectious virus was

1101 quantitated as in Fig. 2A. **C. siRNA specifically reduces NICD1 expression.** Vero rKSHV.294 cells
1102 were transfected with 30pM of the siRNAs described in the legend to Fig. 4A. 48h post transfection,
1103 total cellular proteins were extracted in RIPA buffer, then analyzed via a 10% SDS-PAGE/western blot
1104 as described in the legend to Fig. 1A.

1105
1106

1107 **Fig. 5. Activated Notch binds to KSHV promoters during reactivation.** Triplicate cultures of Vero
1108 rKSHV.294 cells were transfected with empty vector or Rta expression vector in three experiments.
1109 Cross-linked chromatin was sonicated and immunoprecipitated (ChIP'd) with NICD1-specific antibody
1110 or non-specific IgG control. ChIP'd DNA was purified and analyzed by quantitative real-time PCR to
1111 detect sequences located within 1 kb. upstream of the transcriptional start sites of the indicated KSHV
1112 genes. Fold increases in ChIP'd promoters were calculated by the delta-delta Ct method using non-
1113 specific IgG as the internal control for each sample and EV transfection as baseline fold. Folds were
1114 normalized by comparison to NICD1 expression in transfected samples. *$p<0.05$ by t test comparing Rta
1115 to Vec for each primer pair.

1116
1117

1118 **Fig. 6. Activated Notch1 is required for optimal reactivation of KSHV in infected PEL cells. A.**
1119 **DAPT inhibits vDNA accumulation in PEL cells.** Triplicate cultures of KSHV-infected BC3 cells were
1120 treated with vehicle alone ("Vh") or containing 16, 32, or 40 uM DAPT for 65h. Total DNA was purified
1121 using the FlexiGene DNA kit (Qiagen). Intracellular viral DNA was measured by real-time quantitative
1122 (q) PCR using SYBR Green PCR Master Mix (Thermo Scientific) and GAPDH was the internal control.
1123 Fold-DNA was calculated using the ΔCt method and all values were normalized to that of VPA + vehicle
1124 alone, which was set to 100%. *$p<0.03$, **$p<0.009$, and ***$p<0.006$ by t test compared to VPA+Veh.
1125 Results from three biologic replicates were combined. **B. Specific expression of KSHV genes is reduced**

1126 **by Notch inhibition in PEL cells.** Triplicate cultures of KSHV-infected BCBL1 cells were treated with
1127 1 mM VPA and vehicle ("Vh") or DAPT (16, 32, or 40 uM). 48 or 72h post-treatment, ORF59 and K8.1
1128 were detected by indirect immunofluorescence, respectively. The percentages of ORF59 or K8.1 positive
1129 cells were quantitated, and fold-percent positive cells were calculated by normalizing to samples treated
1130 with vehicle alone. Results from three biologic replicates were combined. *p<0.007 and **p<0.005 by t
1131 test compared to VPA+Veh.

1132
1133
1134 **Fig. 7. Ectopic NICD 1-4 are not sufficient to induce KSHV reactivation. A.** Vero rKSHV.294 cells
1135 were transfected with 2.5 ug plasmid DNA expressing each of the indicated proteins and incubated for
1136 72h at which time virus containing media were transferred to 293 MSR tet-OFF cells. Infectious virus
1137 was quantitated as in the legend to Fig. 2A, using the Great EscAPe SeAP kit (Takara). *p<0.0002 by t
1138 test compared to Vec. Data points shown are from one to ten biologic replicates containing two to three
1139 technical replicates for each experimental condition. **B. All four constitutively active Notch isoforms**
1140 **are expressed ectopically in transfected Vero rKSHV.294 cells.** Cells were transfected as in the legend
1141 to Fig 7A, and total proteins were harvested in RIPA buffer 48h later, Western blotted, and probed with
1142 FLAG-tag and tubulin-specific antibodies. All Notch isoforms were observed at the appropriate apparent
1143 MWs (48). **C. Ectopic Notch isoforms 1 and 2 are transactivation competent in Vero rKSHV.294**
1144 **cells.** Triplicate cultures of Vero rKSHV.294 cells were transfected with 0.25 ug of the Notch reporter
1145 plasmid 4xCBS expressing firefly luciferase, control plasmid pcDNA3.1-HisLacZ expressing β-
1146 galactosidase (βgal) and 3 ug of each of the four Notch isoform vectors. Extracts were made 48 h post-
1147 transfection, and raw luciferase values were corrected to β-galactosidase. Folds were calculated by
1148 normalization to samples transfected with luciferase reporter and empty vector (Vec) alone. *p<0.02 and
1149 **p<0.0001 by t test compared to Vec.

1150
1151

1152 **Fig. 8. Ectopic NICD1 cooperates with VPA in KSHV reactivation.** Vero rKSHV.294 cells were

1153 transfected with 1 ug plasmid DNA expressing NICD1 ("N1") or empty vector. 18 h post-transfection,

1154 cells were treated with 1 mM VPA. 72 h post-treatment, virus containing media were transferred to 293

1155 MSR tet-OFF cells. Infectious virus was quantitated as in Fig 2A. *$p<0.05$ by t test.

DeCotiis-Mauro, Han, et al, Fig 1

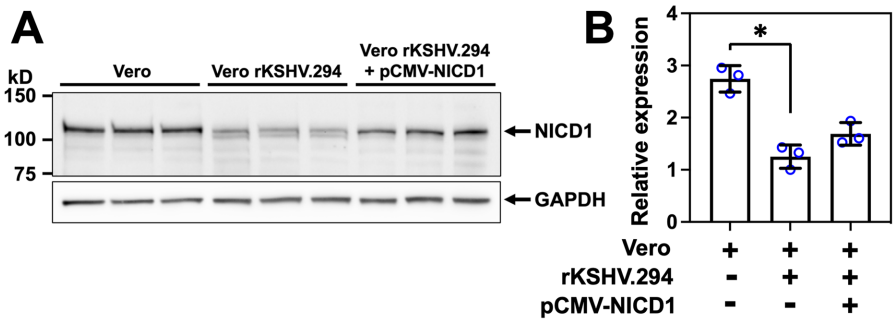

DeCotiis-Mauro, Han, et al Fig 2

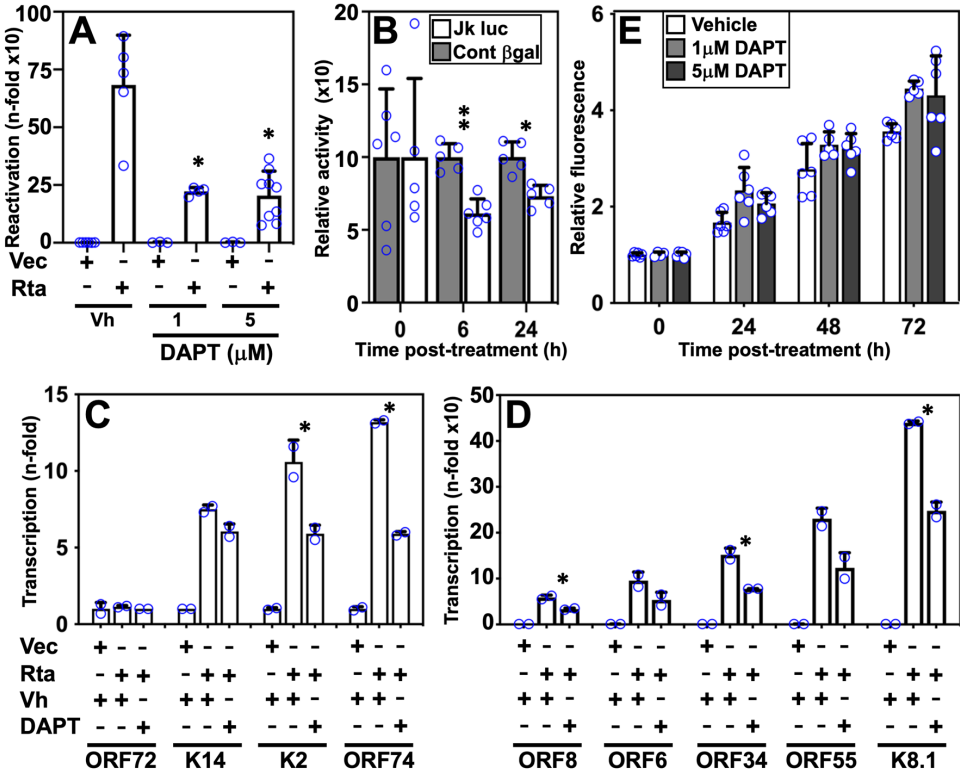

DeCotiis-Mauro, Han, et al, Fig 3

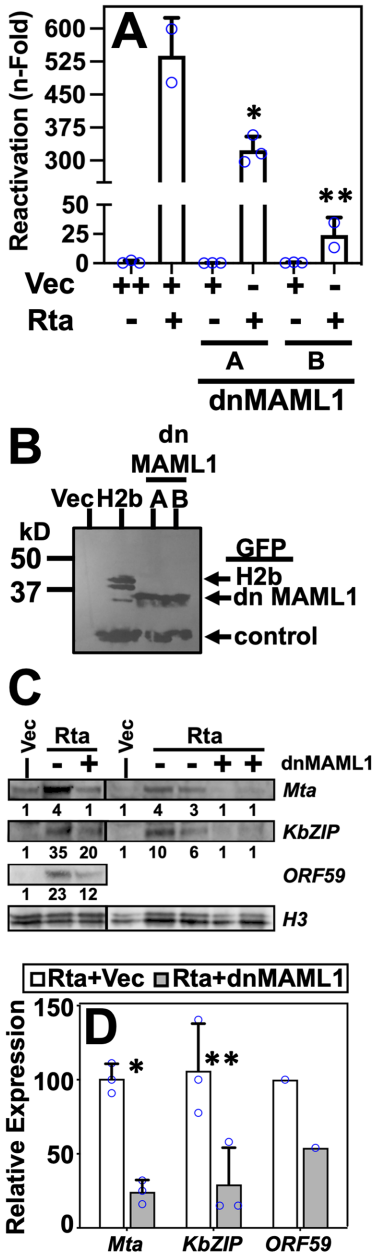

DeCotiis-Mauro, Han, et al Fig 4

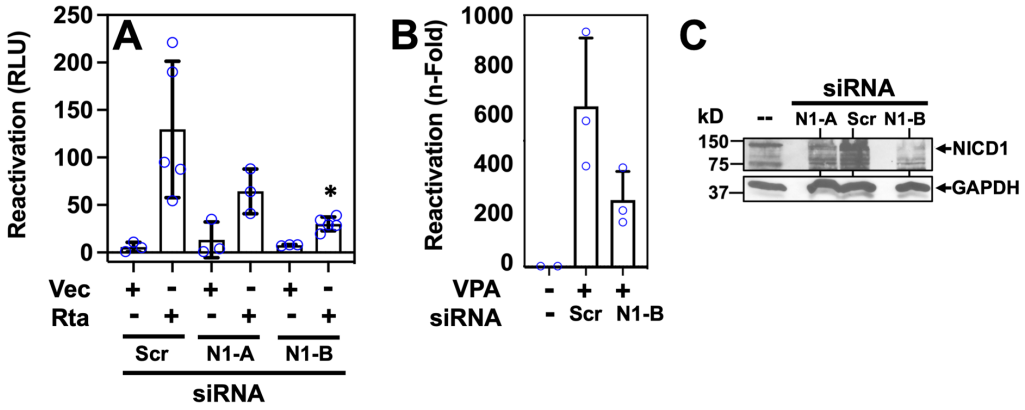

DeCotiis-Mauro, Han, et al, Fig 5

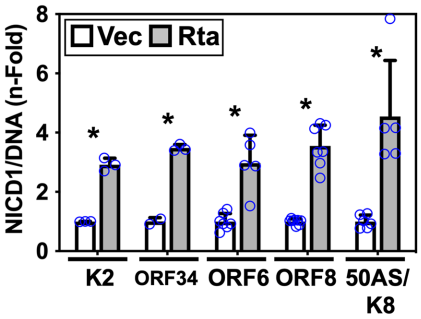

DeCotiis-Mauro, Han, et al Fig 6

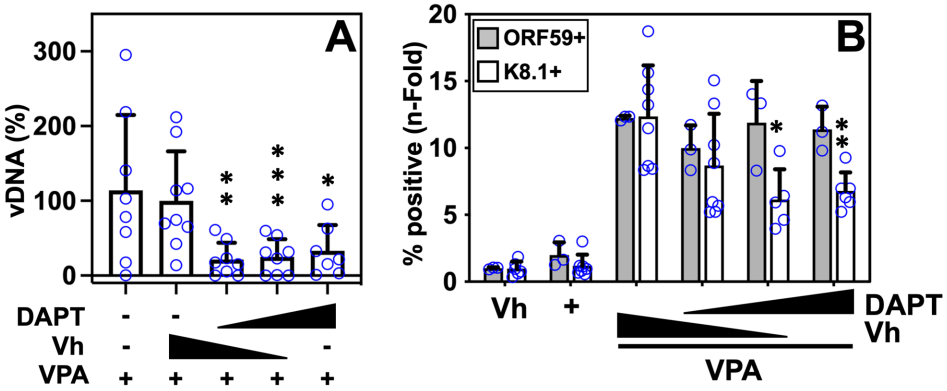

DeCotiis-Mauro, Han, et al, Fig 7

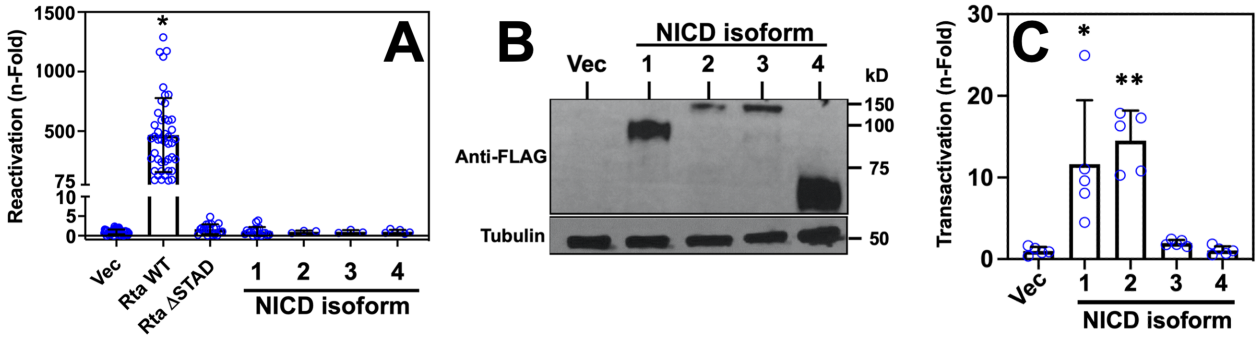
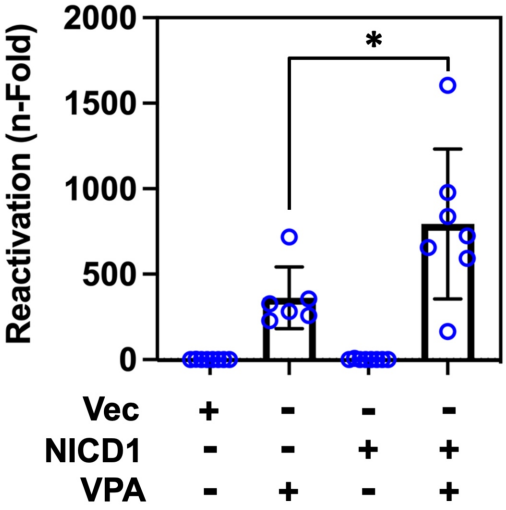
DeCotiis-Mauro, Han, et al, Fig 8